LOAD INDEPENDENT TRAJECTORY CONTROL FOR AN ARTIFICIAL MUSCLE

by

Alper Yaman

B.Sc. in Physics

Boğaziçi University, 2000

Submitted to the Institute of Biomedical Engineering

in partial fulfillment of the requirements

for the degree of

Master of Science

in

Biomedical Engineering

Boğaziçi University

September, 2003

ACKNOWLEDGEMENTS

First and foremost I would like to express my sincere gratitude to my supervisor Associate Professor Mehmed Özkan for the patience, tolerance and helpful criticisms he provided throughout the thesis and also his crucial role in developing my background knowledge and ongoing interest in Robotics.

Furthermore, I am indepted to Professor Yorgo İstefanopulos for his professional support and constructive criticisms.

A heartfell thanks go to my dear friends; Şenol İşçi, Ömer Kocaoğlu, Burhan Öğüt, Gökmen Özer, Burteçin Aksel, Bora Büyüksaraç and Gökhan Işık for their valuable support and friendship they have provided during the thesis, and Mr. Yamanaka, Mr. Terahama and Mr. Negishi from Bridgestone Company from Japan for their technical support and our technician Erhan Uyanık for his support.

My sincere thanks go to my family that has always been there for their endless support, love, and encouragement throughout my whole life.

Last but not least, I would like to thank to my dream girl -Emine- who has always encouraged and supported me to finish my thesis.

ABSTRACT

LOAD INDEPENDENT TRAJECTORY CONTROL FOR AN ARTIFICIAL MUSCLE

In this study, the hysteretic characteristics of pneumatic McKibben artificial muscle were investigated to develop an alternative trajectory control method to traditional PID (Proportional-Integral-Derivative) controller avoiding feedback delays. Furthermore motion trajectory is intended to be payload independent by developing a physical model that will adapt itself to mass changes. In this study, we focus on only one actuator and evaluate our model experimentally. The contraction of the muscle against different pressure values was measured for several different load masses.

The proposed model requires computation of actual forces involved in the motion generation of the muscle. These forces are related to contraction ratio, speed, and acceleration of the actuator. First, the load mass that the muscle lifts is measured by force sensation. The mass assessment is performed by using a friction coefficient model. Next a mathematical model relating actuator pressure with its contraction ratio is established. The coefficients are related to both the load mass and the electrical current speed that controls the servo valve pressure. Because of the spring-like characteristics of the muscle, its contraction ratio is different for different loads for the same control signal. To achieve load independent trajectory control, the physical model must contain mass related parameters. In this control system, control signal (input electrical current) and electrical current speed are related to the target trajectory. The control system is open-loop, and has no feedback.

Keywords: McKibben, artificial muscle, rubbertuator, hysteresis, non-linearity, control.

ÖZET

BİR YAPAY KAS İÇİN YÜKTEN BAĞIMSIZ YÖRÜNGE DENETİMİ

Bu çalışmada geri besleme gecikmelerinden kurtulmak için PID'ye (Proportional-Integral-Derivative) alternatif yeni bir denetim yöntemi geliştirmek amacıyla basınçlı hava ile çalışan McKibben yapay kaslarının histeretik özellikleri araştırıldı. Kütle değişimlerine kendini uyarlayan bir fiziksel model geliştirilerek hareketin yörüngesinin yükten bağımsız olması amaçlandı. Bu çalışmada, bir yapay kas üzerine yoğunlaştık ve modelimizi farklı basınç ve farklı yüklerde kasın kasılması ölçerek oluşturduk.

Öngörülen model kasın hareketi esnasında oluşan kuvvetlerin hesaplanmasını gerektirmektedir. Bu kuvvetler kasın kasılma miktarı, hızı ve ivmesi ile ilişkilidir. İlk olarak, kasın kaldırdığı yükün kütlesi kuvvetler hesaplanarak ölçülür. Sonra da basınç ve kasılma miktarını ilişkilendiren matematiksel model oluşturulur. Katsayılar hem yükün kütlesine, hem de hava basıncını denetleyen elektrik akımının hızına bağlıdır.

Kasın yay benzeri özelliğinden dolayı, aynı denetim sinyali için kasılma oranları farklı kütlelerde farklı olmaktadır. Yükten bağımsız yörünge denetimini geliştirmek için, fiziksel model kütleye bağlı parametreleri içermelidir.

Bu denetim sisteminde, denetim sinyali (elektrik akım girdisi) ve elektrik akım hızı hedef yörüngeyle ilişkilendirilir. Denetim sistemi açık-döngülüdür ve geri beslemeye ihtiyaç duymaz.

Anahtar Sözcükler: McKibben, yapay kas, histeri, doğrusal olmayan sistemler, denetim.

TABLE OF CONTENTS

ACKNOWLEDGEMENTS iii
ABSTRACT iv
ÖZET v
LIST OF FIGURES vii
LIST OF SYMBOLS xi
LIST OF ABBREVIATIONS xiii
1. INTRODUCTION 1
2. THEORETICAL BACKGROUND 4
2.1 Pantographic Structure of Rubbertuator 5
2.2 Spring-like Characteristic of the Rubbertuator 6
2.3 Rubbertuator Contraction Ratio 6
2.4 Force, Pressure and Contraction Ratio Relations of Rubbertuator . . . 7
2.5 Rubbertuator Frictional Forces 8
2.6 Rubbertuator Power to Weight Ratio 8
2.7 Antagonistic Muscle Pair 9
3. SYSTEM ARCHITECTURE 10
3.1 HARDWARE 10
3.2 HARDWARE CALIBRATION: 16
3.3 SOFTWARE 17
4. METHOD 20
4.1 FRICTIONAL FORCE COEFFICIENT MODEL 20
4.2 PRESSURE-CONTRACTION RATIO MODEL 38
4.3 INVERSE KINEMATICS MODEL IN LABVIEW 54
5. CONCLUSIONS AND DISCUSSIONS 59
REFERENCES 61

LIST OF FIGURES

Figure 2.1	The conversion of the pressure forces to tensional forces on threads.	5
Figure 3.1	The experimental setup.	10
Figure 3.2	The setup: muscle at rest.	11
Figure 3.3	The setup: contracted muscle.	11
Figure 3.4	Servo valve circuitry diagram [5].	12
Figure 3.5	Pressure vs input electrical current graph [5].	13
Figure 3.6	Servo valve pin connection [5].	13
Figure 3.7	The three channels of optical encoder.	14
Figure 3.8	Connection of the encoder to the counters.	16
Figure 4.1	Forces generated by rubbertuator.	20
Figure 4.2	Chi-square Modeling: Coefficient of friction vs contraction ratio for 5.6 mA/sec current speed. Blue: experimental data, red: model's values.	23
Figure 4.3	Chi-square Modeling: Coefficient of friction vs contraction ratio for 6.7 mA/sec current speed. Blue: experimental data, red: model's values.	23
Figure 4.4	Chi-square Modeling: Coefficient of friction vs contraction ratio for 8.3 mA/sec current speed. Blue: experimental data, red: model's values.	24
Figure 4.5	Chi-square Modeling: Coefficient of friction vs contraction ratio for 11.1 mA/sec current speed. Blue: experimental data, red: model's values.	24
Figure 4.6	Chi-square Modeling: Coefficient of friction vs contraction ratio for 16.7 mA/sec current speed. Blue: experimental data, red: model's values.	25
Figure 4.7	Fifth Order Polynomial Modeling: Coefficient of friction vs contraction ratio for 5.6 mA/sec current speed. Blue: experimental data, red: model's values.	26

Figure 4.8 Fifth Order Polynomial Modeling: Coefficient of friction vs contraction ratio for 6.7 mA/sec current speed. Blue: experimental data, red: model's values. 27

Figure 4.9 Fifth Order Polynomial Modeling: Coefficient of friction vs contraction ratio for 8.3 mA/sec current speed. Blue: experimental data, red: model's values. 27

Figure 4.10 Fifth Order Polynomial Modeling: Coefficient of friction vs contraction ratio for 11.1 mA/sec current speed. Blue: experimental data, red: model's values. 28

Figure 4.11 Fifth Order Polynomial Modeling: Coefficient of friction vs contraction ratio for 16.7 mA/sec current speed. Blue: experimental data, red: model's values. 28

Figure 4.12 1st Coefficient of Fifth Order Polynomial Modeling: 1st Polynomial Coefficient vs current speed. 29

Figure 4.13 2nd Coefficient of Fifth Order Polynomial Modeling: 2nd Polynomial Coefficient vs current speed. 30

Figure 4.14 3rd Coefficient of Fifth Order Polynomial Modeling: 3rd Polynomial Coefficient vs current speed. 30

Figure 4.15 4th Coefficient of Fifth Order Polynomial Modeling: 4th Polynomial Coefficient vs current speed. 31

Figure 4.16 5th Coefficient of Fifth Order Polynomial Modeling: 5th Polynomial Coefficient vs current speed. 31

Figure 4.17 6th Coefficient of Fifth Order Polynomial Modeling: 6th Polynomial Coefficient vs current speed. 32

Figure 4.18 Superpositional modeling of the coefficient of friction with respect to contraction ratio. 33

Figure 4.19 Dependence of $f_1(v^2)$ on current speed. Blue curve: experimental data, Red line: linear fit, and Green curve: quadratic fit to the experimental data. 33

Figure 4.20 Coefficient of friction vs contraction ratio for all electrical current speed values for the contraction of the muscle. Blue: experimental data, red: model's values. 34

Figure 4.21 Contraction of the muscle: Coefficient of friction vs contraction ratio for 5.6 mA/sec current speed. Blue: experimental data, red: model's values. 35

Figure 4.22 Contraction of the muscle: Coefficient of friction vs contraction ratio for 6.7 mA/sec current speed. Blue: experimental data, red: model's values. 35

Figure 4.23 Contraction of the muscle: Coefficient of friction vs contraction ratio for 8.3 mA/sec current speed. Blue: experimental data, red: model's values. 36

Figure 4.24 Contraction of the muscle: Coefficient of friction vs contraction ratio for 11.1 mA/sec current speed. Blue: experimental data, red: model's values. 36

Figure 4.25 Contraction of the muscle: Coefficient of friction vs contraction ratio for 16.7 mA/sec current speed. Blue: experimental data, red: model's values. 37

Figure 4.26 Standard Deviation in Coefficient of friction vs current speed. 37

Figure 4.27 Superpositional Modeling of the pressure with respect to contraction ratio. 38

Figure 4.28 The shift of the curve related to the mass and the electrical current speed. 39

Figure 4.29 a_1 with respect to current speed for 11.1380 kg mass. 41

Figure 4.30 a_2 with respect to current speed for 11.1380 kg mass. 41

Figure 4.31 b_0 with respect to current speed for 11.1380 kg mass. 42

Figure 4.32 b_4 with respect to current speed for 11.1380 kg mass. 42

Figure 4.33 Standard deviation of the modeled pressure for contraction with respect to electrical current speed for 11.1380 kg mass. 43

Figure 4.34 Standard deviation of the modeled pressure for relaxation with respect to electrical current speed for 11.1380 kg mass. 43

Figure 4.35 Coefficient a_0 (kgf/m^2) for contraction related to mass (kg). Blue: experimental data, red: model's values. 45

Figure 4.36 Coefficient a_1^0 (kgf/m^2 sec/mA) for contraction related to mass (kg). Blue: experimental data, red: model's values. 46

Figure 4.37 Coefficient a_1^1 (kgf/m^2) for contraction related to mass (kg). Blue: experimental data, green: model's values. 46

Figure 4.38 Coefficient a_2^0 (kgf/m^2 sec/mA) for contraction related to mass (kg). Blue: experimental data, green: model's values. 47

Figure 4.39 Coefficient a_2^1 (kgf/m^2) for contraction related to mass (kg). Blue: experimental data, green: model's values. 47

Figure 4.40 Coefficient a_3 (kgf/m^2) for contraction related to mass (kg). Blue: experimental data, red: model's values. 48

Figure 4.41 Coefficient a_4 (kgf/m^2) for contraction related to mass (kg). Blue: experimental data, red: model's linear values, green: model's quadratic values. Linear values are used in model 48

Figure 4.42 Coefficient b_0^0 (kgf/m^2 sec/mA) for relaxation related to mass (kg). Blue: experimental data, red: model's values. 50

Figure 4.43 Coefficient b_0^1 (kgf/m^2) for relaxation related to mass (kg). Blue: experimental data, red: model's values. 51

Figure 4.44 Coefficient b_1 (kgf/m^2) for relaxation related to mass (kg). Blue: experimental data, red: model's values. 51

Figure 4.45 Coefficient b_2 (kgf/m^2) for relaxation related to mass (kg). Blue: experimental data, red: model's values. 52

Figure 4.46 Coefficient b_3 (kgf/m^2) for relaxation related to mass (kg). Blue: experimental data, red: model's values. 52

Figure 4.47 Coefficient b_4^0 (kgf/m^2 $(sec/mA)^2$) for relaxation related to mass (kg). Blue: experimental data, red: model's values. 53

Figure 4.48 Coefficient b_4^1 (kgf/m^2 sec/mA) for relaxation related to mass (kg). Blue: experimental data, red: model's values. 53

Figure 4.49 Coefficient b_4^2 (kgf/m^2) for relaxation related to mass (kg). Blue: experimental data, red: model's values. 54

Figure 4.50 Error map of the target contraction ratio for the target 0 contraction speed (meter per second). 58

Figure 4.51 Error map of the target contraction ratio speed for the target 0 contraction speed (meter per second). 58

LIST OF SYMBOLS

F	Force
$F_{generated}$	Generated Force
$F_{friction}$	Frictional Force
N	Normal Force
$S_{contact}$	Area of the Contact Surface
P	Pressure
$\dot{P}$	Pressure Speed
A	Area
b	The Length of the Thread
l_0	Initial Length of the Muscle
l	The Length of the Muscle
n	Number of Turns of a Thread
D	Diameter of the Muscle
r_0	Initial Radius of the Muscle
f	Coefficient of Friction
k	Correction Factor
g	Gravitational Acceleration
ν	Electrical Current Speed
m	Mass of the Load
f_0, f_1, f_2, f_3	Coefficients of the Frictional Force Coefficient Model
$p_0, p_1, p_2, p_3, p_4, p_5$	Polynomial Model Coefficients
a_0, a_1, a_2, a_3, a_4	Coefficients of the Pressure-Contraction Ratio Model for Contractio
b_0, b_1, b_2, b_3, b_4	Coefficients of the Pressure-Contraction Ratio Model for Relaxation
a_0^0, a_0^1	Coefficients of a_0
a_1^0, a_1^1	Coefficients of a_1
$a_1^{00}, a_1^{01}, a_1^{02}, a_1^{03}$	Coefficients of a_1^0
$a_1^{10}, a_1^{11}, a_1^{12}$	Coefficients of a_1^1
a_2^0, a_2^1	Coefficients of a_2

$a_2^{00}, a_2^{01}, a_2^{02}$	Coefficients of a_2^0
$a_2^{10}, a_2^{11}, a_2^{12}$	Coefficients of a_2^1
a_3^0, a_3^1	Coefficients of a_3
a_4^0, a_4^1	Coefficients of a_4
b_0^0, b_0^1	Coefficients of b_0
b_0^{00}, b_0^{01}	Coefficients of b_0^0
b_0^{10}, b_0^{11}	Coefficients of b_0^1
b_1^0, b_1^1	Coefficients of b_1
b_2^0, b_2^1	Coefficients of b_2
b_3^0, b_3^1	Coefficients of b_3
b_4^0, b_4^1, b_4^2	Coefficients of b_4
b_4^{00}, b_4^{01}	Coefficients of b_4^0
b_4^{10}, b_4^{11}	Coefficients of b_4^1
b_4^{20}, b_4^{21}	Coefficients of b_4^2
α	The Angle between the Thread and the Muscle Axis
ε	Contraction Ratio
$\dot{\varepsilon}$	Contraction Speed

LIST OF ABBREVIATIONS

EPV	Electromagnetic Proportion Valve
PID	Proportional Integral Derivative
ANN	Artificial Neural Network

1. INTRODUCTION

Artificial muscles, especially McKibben muscles used in both industry and biomedical engineering have overwhelming benefits as compared to other actuators like servo motors. Their high power-to-weight ratio is one of them, which provides us to make compact robots. These muscles also do not require step adjustments as in the servo motors. McKibben muscles, also known as rubbertuators, can be controlled by small electrical currents, ranging from 4 mA to 20 mA by servo valve units. These units include operational amplifier, pressure sensor and a feedback control system of their own to control the air supply precisely. 0.5 to 5 atm air pressure is enough to generate the force by a rubbertuator. As the air is supplied into the rubbertuator, the rubber inner tube inside the rubbertuator inflates and forces the braided shell threads to contract over the muscle. Most of the force generated by the inner tube can be converted to the tensional force on the threads due to their pantographic arrangement. Since there is a frictional force between the inner tube and the threads and between the threads themselves, the muscle characteristics have hysteresis.

Although design of new pneumatic systems, such as rubbertuator, becomes increasingly important and preferable, due to their excellent power-weight performance and good compliance, there are problems with their control due to the non-linearities in values, the compliance of the fluid medium, and hysteresis. Systems to control those pneumatic actuators have primarily been based on traditional PID (Proportional-Integral-Derivative) or similar techniques. Since these control techniques have feedback loop, and the response is delayed the control scheme could easily become unstable [1].

In the Robotics Laboratory of the Institute of Biomedical Engineering at Bogazici University, there is a Bridgestone robot arm having four degrees of freedom. All the joints are actuated by antagonistic muscle pairs. Hence, achieving a precise modeling of a muscle is the most important part of the project to control the whole robot arm.

The aim of this thesis is to model the muscle's response against the applied pressure and to control the trajectory of the muscle without load dependence. The muscle has spring-like characteristics. Therefore, its response to the applied pressure changes with the load. As the mass of the load increases, the maximum contraction ratio decreases. The experiments and the developed LabView program are designed to find the coefficients of the model so that precise control can be reached.

To develop a control method that is based on a physical model of a pneumatic actuator, rubbertuator so that no feedback loops will be needed, two sets of parameters related to

1. Rubbertuator thread friction,
2. The contraction ratio and pressure.

The thread frictional force is the addition of the friction between the textile threads and friction between the threads and the inner tube. The friction in textile fibres is modeled with various types of mathematical relations. Three of them are as below:

$$F = \mu_0 N + \alpha S \tag{1.1}$$

$$F/N = A - B \log N \tag{1.2}$$

$$F = \alpha N + bN^c \tag{1.3}$$

where S is the area of the contact, μ_0, α, A, B, a, b, and c are constants and N is the normal force [2]. The frictional force can be calculated from data and modeled as the empirical formulas above. Lagrangian equation of the system enables the program to find out the mass of the load if the frictional force is modeled.

The relation between the pressure and the contraction ratio is fitted to a function related to the frequency or the speed of the input current and the mass of the load. If the fitting is successful, the target trajectory of the muscle can be reached by measuring the input pressure due to the fitted formula.

The McKibben muscle is not only used in industry but also in biomedical engineering. It is useful to make soft prosthesis. However, there are two disadvantages of the McKibben muscle for these applications. First, the pressurized air is contained in a big tank. This restricts the mobility of the systems actuating by McKibben muscle. Second, the nonlinear behavior of that muscle depends on a number of parameters including humidity, temperature, load etc. Because of this, it is hard to make precise modeling of the muscle. Precise control systems for the muscle have been developed with PID (Proportional-Integral-Derivative) or neural network, but the feedback in that systems slows down the control of the muscle. If a mathematical model of the muscle is verified or found experimentally, it can be more useful than PID or neural network since it does not have any feedback loop.

In the Chapter 2, a general information about the McKibben muscles is given. In the Chapter 3, the structure of the McKibben muscles and their characteristic behavior is explained. In Chapter 4, parts of the setup and their features are explained. In Chapter 5, it is explained how to make the calibration of the system was made, how the data is collected and processed. In Chapter 6, the model is explained and the results are given. In Chapter 7, results of the study are discussed and the further studies are suggested.

2. THEORETICAL BACKGROUND

McKibben muscle was invented to motorize pneumatic arm orthotics in the 1950s by physician Joseph L. McKibben. It was aimed to control handicapped hands [3]. Bridgestone Company then realized the importance of such an artificial muscle and redesigned it to be used in painting robots.

McKibben muscle, which is also called rubbertuator (rubber-actuator) for its inner rubber tube, works with pressurized air. The air pressure forces the rubber inner tube inside the muscle to expand. The pressure generates radial force in the direction of expansion. This radial force is converted to tensional force on each non-extensible thread. Ideally, there is no frictional force between the inner tube and the threads, but in reality, there is frictional force which is made up of static and dynamic friction components.

Thermodynamically, the expansion of the gas is a complex phenomenon inside the inner tube. As both the pressure and the volume are increased, temperature also changes infinitesimally. All these changes have influence on the generated force. As the volume of the inner tube increases, the total surface area increases. So, due to the Equation 2.1, the total generated force increases. As the expansion slows down, the force generation declines with exponential-like behavior.

$$F = \int \int dP dA \tag{2.1}$$

where, F is the force, dP is the pressure and dA is the area.
As mentioned earlier, this force is converted to tensional force by the threads on each point of the pantograph as shown in Figure 2.1.

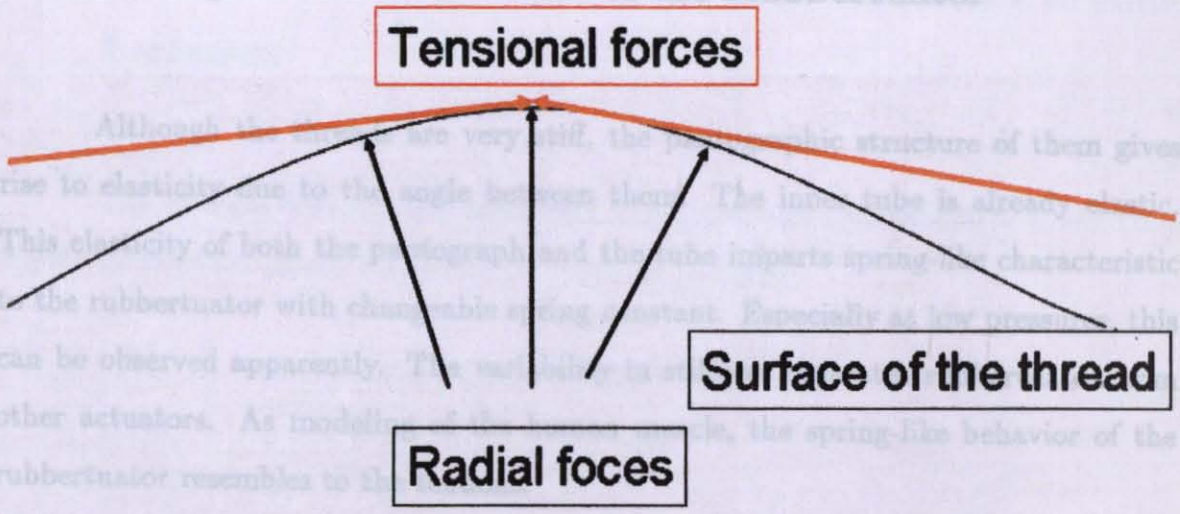

Figure 2.1 The conversion of the pressure forces to tensional forces on threads.

2.1 Pantographic Structure of Rubbertuator

The rubbertuator contains the braided threads turning around the tube with a definite initial angle α_0. As the length of the threads is constant, due to the Pythagorean theorem, this angle relates the length of the muscle with its diameter as in Equations 2.2 and 2.3. This angle has an important role in converting the axial force to tensional force [4].

$$b^2 = l^2 + (n\pi D)^2 \tag{2.2}$$

$$\tan(\alpha) = \frac{(n\pi D)}{l} \tag{2.3}$$

where, b is the thread length, l is the length of the muscle, n is the number of turns of a thread, D is diameter of the muscle, and α is the angle between the thread and the muscle axis.

2.2 Spring-like Characteristic of the Rubbertuator

Although the threads are very stiff, the pantographic structure of them gives rise to elasticity due to the angle between them. The inner tube is already elastic. This elasticity of both the pantograph and the tube imparts spring-like characteristic to the rubbertuator with changeable spring constant. Especially at low pressures, this can be observed apparently. The variability in stiffness separates rubbertuator from other actuators. As modeling of the human muscle, the spring-like behavior of the rubbertuator resembles to the tendons.

2.3 Rubbertuator Contraction Ratio

As the rubbertuator contracts in length and expands in diameter, the cylindrical shape of the muscle degenerates. Since the two ends of the muscle are fixed by metal fitting, a conical shape occurs at these ends. This requires a correction factor to the contraction ratio.

Contraction ratio is the relative change in the length of the muscle related to its initial length. Its maximum value is around 0.30. However, the excess of 0.20 can cause damage on rubbertuator [5].

$$\varepsilon = \frac{(l_0 - l)}{l_0} \tag{2.4}$$

where, ε is contraction ratio, l is the length of the muscle, l_0 is the initial length of the muscle.

2.4 Force, Pressure and Contraction Ratio Relations of Rubbertuator

The relation between the generated force, pressure and contraction force has shown by the force generator model of Tondu & Lopez [3].

$$F(\varepsilon, P) = (\pi r_0^2) P[a(1-\varepsilon)^2 - b] \tag{2.5}$$

$$a = \frac{3}{\tan^2(\alpha_0)} \tag{2.6}$$

$$b = \frac{1}{\sin^2(\alpha_0)} \tag{2.7}$$

where, F is generated force, P is pressure, r_0 is the initial radius of the muscle, and α_0 is the initial angle between the thread and the rubbertuator axis.

The generated force is independent of the initial length. It is directly proportional to the pressure and the initial cross-sectional area.

As mentioned above, the correction factor must be included to compensate for the conical shape at the two ends of the muscle. So the formula becomes:

$$F(\varepsilon, P) = (\pi r_0^2) P[a(1-k\varepsilon)^2 - b] \tag{2.8}$$

in which k is the correction factor. As seen in the Formula 2.8; when pressurized air is given, at the initial state the contraction force is zero and the force has its maximum value. In an opposing manner, at the final state, the contraction ratio reaches its maximum value while the force decrease to zero. The decrease of the force gives

smoothness in movement.

$$F_{max} = (\pi r_0^2) P[a - b] \tag{2.9}$$

$$\varepsilon_{max} = \frac{1}{k}[1 - \sqrt{\frac{b}{a}}] \tag{2.10}$$

2.5 Rubbertuator Frictional Forces

During the contraction, the threads stay almost rigidly locked with the inner tube, and it is assumed that the pressure force is fully transmitted to the threads. The friction between the inner tube and the threads is small as compared to the friction between the threads. The movement of the threads to expand causes the friction. Variation of contact surface among the threads and the changing stickiness makes this frictional force dependent on both the contraction ratio and contraction speed. The frictional force, considered by Tondu and Lopez, consists of static and kinetic parts. The expression for static friction is given in [3] by the Equation:

$$|F_{static\ dry\ friction}| = f_s S_{contact} P \tag{2.11}$$

where $S_{contact}$ is the area of the contact surface, P is the pressure. During the contraction, the pantograph opens and the contact surface decreases [3].

2.6 Rubbertuator Power to Weight Ratio

Power to weight ratio is a simple but important method to compare the actuators. Rubbertuators are very soft as compared to other pneumatic devices. The successful conversion of the pressure to tensional force enables them to have high power per weight.

2.7 Antagonistic Muscle Pair

The free ends of the two rubbertuators are connected by a chain around a wheel of radius R while the other ends are fixed. This antagonism is based on biceps-triceps muscle system in human body. In this system, the rubbertuators are initially at the same pressure P_0. It is logical to increase one of them by ΔP (pressure difference) while decreasing the other's by the same pressure difference to obtain symmetrical actuation.

In this manner, the modeling of the human muscle can be achieved. Since the influence of the frictional forces is diminished, the control of the motion in two directions can be obtained.

3. SYSTEM ARCHITECTURE

An experimental setup was built to test the proposed control model. In this chapter, the developed system architecture components are described in detail.

3.1 HARDWARE

The setup is built on a wooden board. Figure 3.1 shows the connections of the hardware. One end of the rubbertuator is fixed as the other is linked to a load. As the experiments are carried out, the rubbertuator lifts the load by the applied pressure.

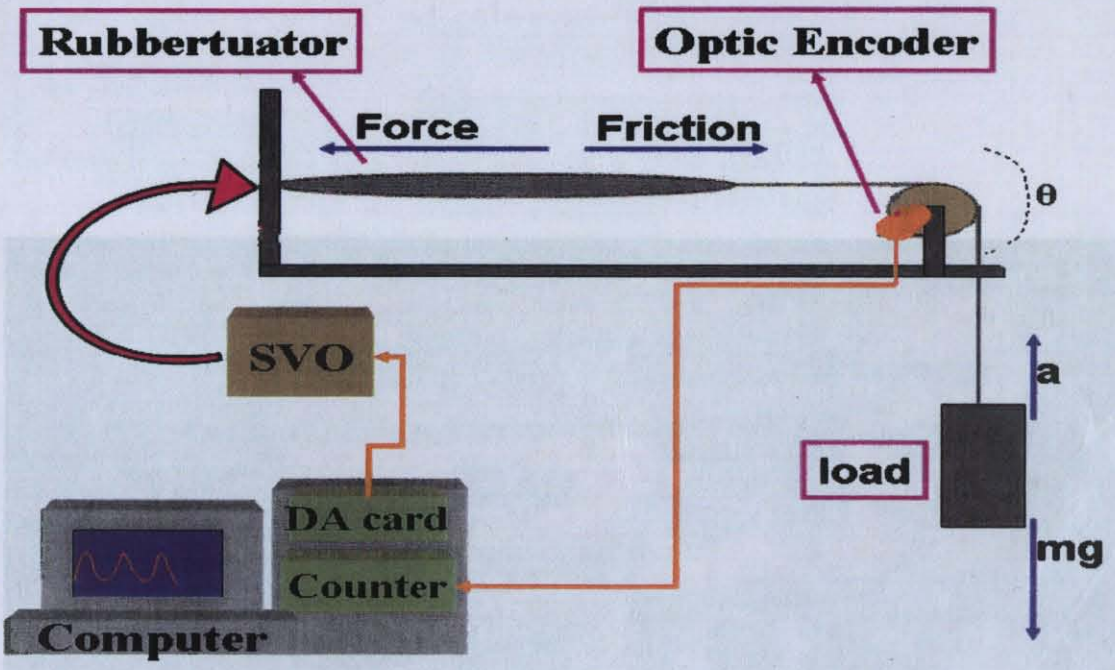

Figure 3.1 The experimental setup.

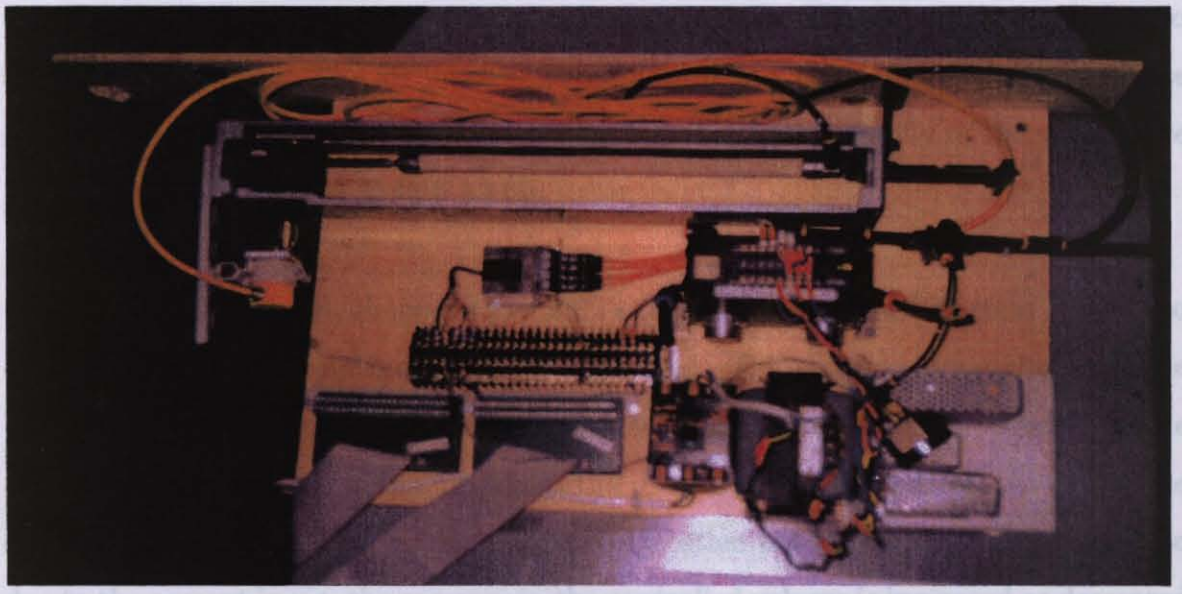

Figure 3.2 The setup: muscle at rest.

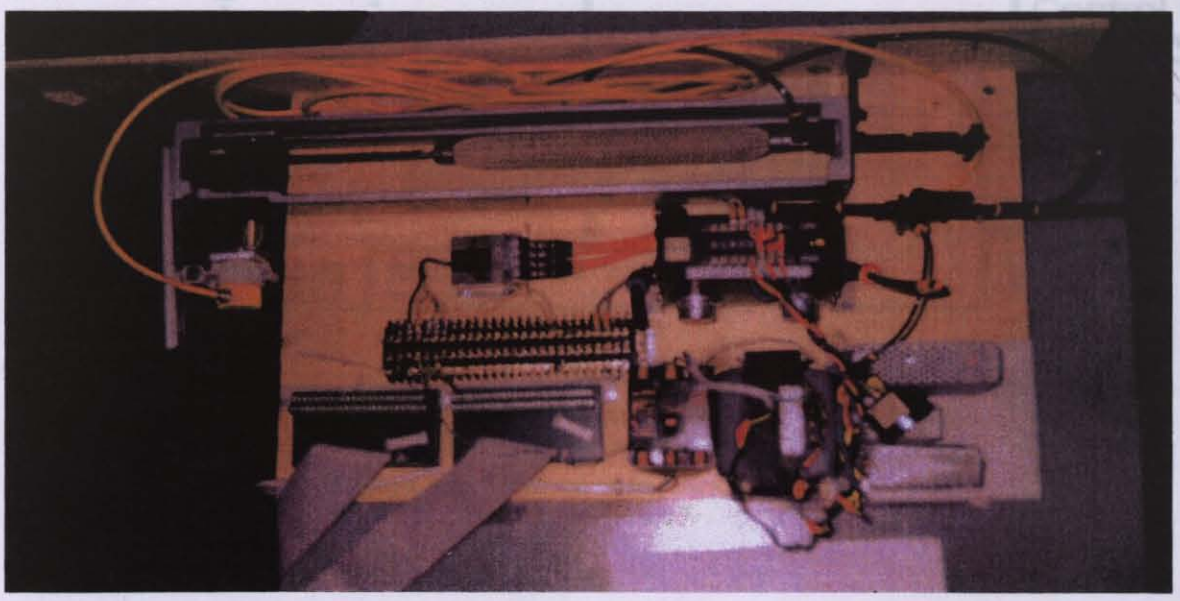

Figure 3.3 The setup: contracted muscle.

Servo Valve: Servo valve is the unit that enables the experimenters to control the pressure of the air by electrical current input. The current input should be between 4 mA and 20 mA. Servo valve has two separate channels. The air supply can be up to 6 bar pressurized air. The air must be dehumidified and clean in order to expand the lifespan of the rubbertuator as much as possible. The power supply of the servo valve is +15 V (0.5 A) and -15 V (0.1 A) [5].

For each channel, there are two EPVs (Electromagnetic Proportion Valves) to control the amount of air supplied and exhausted. The system simply compares the input signal with the signal received from the pressure sensor in the servo valve. Inside the servo valve, there is a volume where the pressure is under control. As one of the electromagnetic proportion valves is opened, the other one is closed synchronously. So due to the current input, the pressure in the controlled volume is increased or decreased [5]. Figure 3.4 shows the Servo valve's circuitry diagram inside:

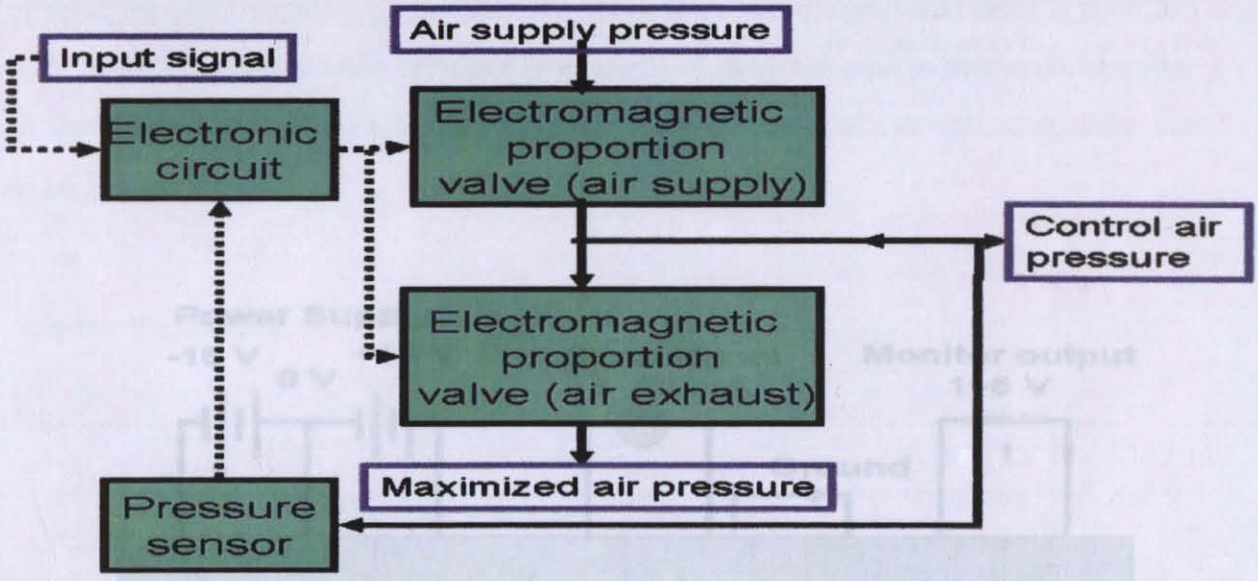

Figure 3.4 Servo valve circuitry diagram [5].

The controlled pressure is linearly proportional to the electrical current input between 4 mA and 20 mA. The normal characteristics of the servo valve and the servo valve pin connections are as in Figures 3.5 and 3.6:

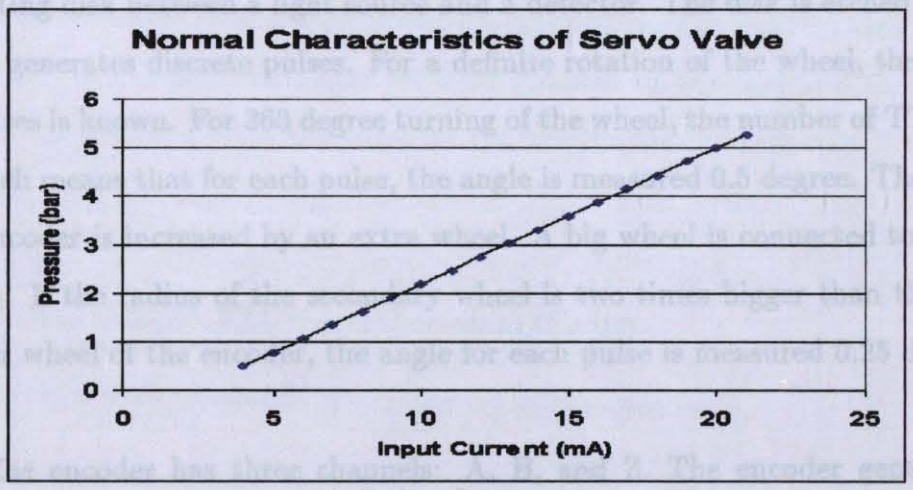

Figure 3.5 Pressure vs input electrical current graph [5].

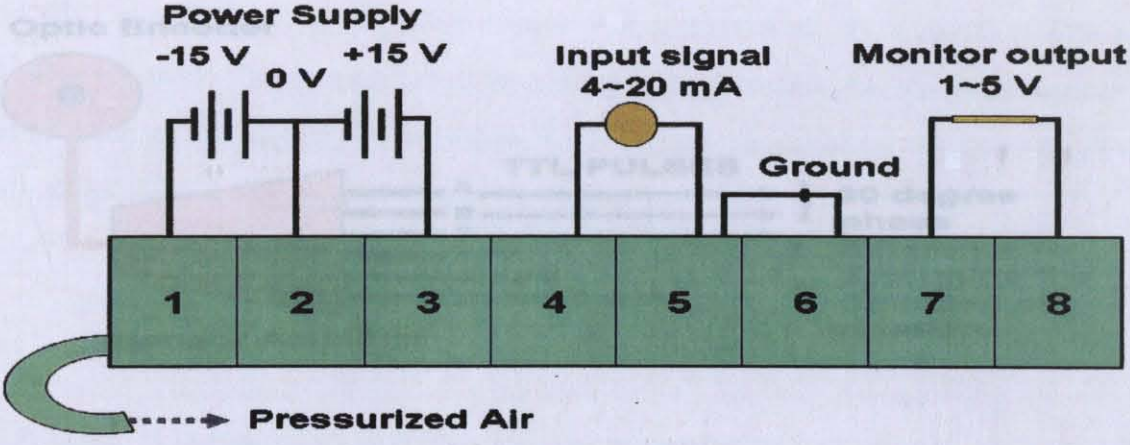

Figure 3.6 Servo valve pin connection [5].

Optical Encoder: An optical encoder(FEC-4B0720-SV DuPont) and a sensor amplifier (SAM-200B01 DuPont) are used to measure the angle that the joint rotates. The voltage supply is +5V DC and the output signal is TTL. Inside the encoder, there is a rotating disk between a light source and a detector. The disk is etched so that the detector generates discrete pulses. For a definite rotation of the wheel, the number of TTL pulses is known. For 360 degree turning of the wheel, the number of TTL pulses is 720, which means that for each pulse, the angle is measured 0.5 degree. The resolution of the encoder is increased by an extra wheel. A big wheel is connected to the axis of the joint. If the radius of the secondary wheel is two times bigger than the radius of the outer wheel of the encoder, the angle for each pulse is measured 0.25 degree.

The encoder has three channels: A, B, and Z. The encoder generates three separate TTL signals from these channels. There is an 90 degree phase difference between A and B channels. A leads B by this phase difference so that the direction of rotation is determined. A single pulse appears once per revolution from Z channel. This common pulse is used to adjust the origin of the joint and to count the number of the revolutions. The pin connections and three channels of the optical encoder are as in Figure 3.7:

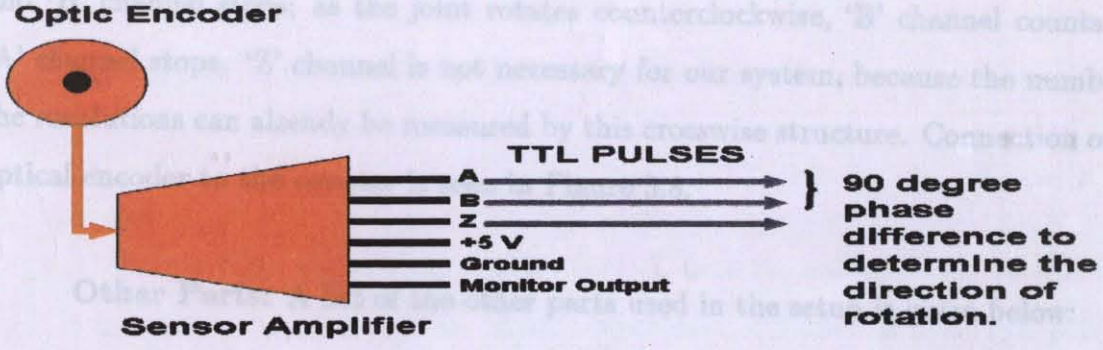

Figure 3.7 The three channels of optical encoder.

Digital to Analog Converter: National Instruments' PC-AO-2DC digital-to-analog converter card is used to supply electrical current input to the servo valves.

The output of the card is 0-20 mA current. The card has two channels, therefore one card can be used to drive both channels of the servo valve.

Counter: National Instruments' PC-TIO-10 card is used to count the TTL signal output of the encoder. There are eight counters on the card and all of them can be driven separately. Two of the counters are used in the experiments. A counter has three pins:

1. source: The input TTL signal is given to this pin.
2. gate: It is used to control the triggering of the counter.
3. out: It is used to generate signal by the counter. This pin is not necessary for our study.

'A' channel of the optical encoder is connected to the source of the first counter and to the gate of the second one, 'B' channel of the optical encoder is connected to the source of the second counter and to the gate of the first one. By this crosswise connection and the phase difference of 90 degree between 'A' and 'B' channels, a counter can be triggered by the other one. As the joint rotates clockwise, 'A' channel counts and 'B' channel stops; as the joint rotates counterclockwise, 'B' channel counts and 'A' channel stops. 'Z' channel is not necessary for our system, because the number of the revolutions can already be measured by this crosswise structure. Connection of the optical encoder to the counter is seen in Figure 3.8.

Other Parts: A list of the other parts used in the setup is given below:

- Load: It is connected to free end of the rubbertuator.
- Ports and Cables: They are necessary to connect the cards to servo valve and optical encoder.
- Transformer and AC-DC Converter: It is needed to supply +15 and -15 V DC to the servo valve and +5 V DC to the optical encoder.

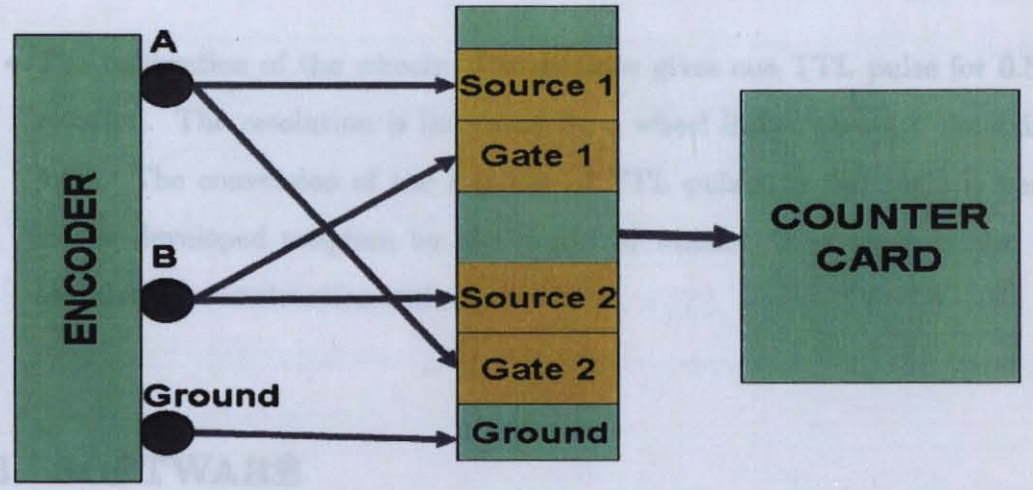

Figure 3.8 Connection of the encoder to the counters.

- Pressure Sensor: The adjustment of the servo valve is made by observing the pressure of the air by a pressure sensor.

3.2 HARDWARE CALIBRATION:

The following calibrations are necessary for before the data is started to collect and the software is developed:

- The servo valve calibration: Calibration of the servo valve is done by the "zero" adjustment trimmer and the "span" adjustment trimmer on the right side of it. It is necessary to adjust the minimum and maximum limit of the pressure. By adjusting the zero to 0.5 bar and the span to 5 bar, it is guaranteed that the pressure cannot exceed these limits.
- The optical encoder calibration: The optical encoder is actually generates dummy voltage values up to 100 milivolts. But the counter needs TTL signals to count. By consulting the BridgeStone engineers, this problem has been handled. The

3 kΩ-0.5 W resistances are connected between the +5 volts power supply of the encoder and A, B and Z phase. Doing this, the encoder starts to give TTL signals.

- The calibration of the wheels: The encoder gives one TTL pulse for 0.5 degree rotation. The resolution is increased by a wheel linked through the axis of the joint. The conversion of the number of TTL pulses to the angle is performed in the developed program by the radius of wheels. This angle is also used to calculate the contraction ratio.

3.3 SOFTWARE

LabView is the software that is used to communicate DA card and the counter. Its powerful graphical interface hierarchy allows the users to make programs quickly. The library is developed in LabView environment, which includes numbers of vi.s (LabView files) to collect data and to control hardware.

Data Acquisition: The developed program to take data includes these steps:

1. Resetting of the Cards: Before taking data, both cards are reset to avoid the errors resulting from previous measurements.

2. Configuring the Cards: The cards are configured by a data acquisition in-built .dll file of the LabView and the signal array of the electrical current is produced.

3. Running the Cards: The DA card sends the electrical current signals ranging from 0 to 20 mA to the servo valve so that the pressure of the air can be changed. As the pressure is changed and the rubbertuator contracts or relaxes, the wheel of the encoder is rotated by the wheel on the joint. As it is rotated, it produces TTL pulses. The counter counts those TTL pulses and the developed program calculates the angle that the joint rotates.

4. Conversions: The TTL pulses are used to calculate the angle, the contraction

ratio, the contraction speed, and the contraction acceleration. The electrical current signals that are transmitted to the servo valve are also used to calculate the pressure. The characteristics of the servo valve are known, and the conversion of the electrical current signal to pressure is linear as indicated in the BridgeStone's Operational Manual.[5] The servo valve converts the electrical current signals to pressure by an in-built operational amplifier.

5. Saving of the Data: The electrical current signal, contraction ratio, contraction speed, and contraction acceleration values are saved in ASCII format so that they can be processed in other environment.

Data Collection Procedure: The sinusoidal signal of the electrical current is applied to the servo valve in the full range (From 0 to 20 mA).The electrical current speed which is proportional to the frequency of the signal is changed approximately from 5.6 to 16.7 mA/sec. The time delay between the samples are 12 msec. If the electrical current speed is selected above 16.7 mA/sec, the transmission of the signal is faster than the contraction time of the muscle. To allow the muscle to contract with the signal synchronously, the data is taken in this range. Taking data below 5.6 mA/sec is not necessary, because the muscle contracts very slowly. For each current speed, the data is taken by five sinusoidal waveforms. For twenty different current speeds, the data set of current and the contraction ratio is taken.

The measurement of the number of counts is synchronous with the transmission of the signal. The number of counts is converted to angle and contraction ratio. The contraction speed and the contraction acceleration are calculated, and the signal is converted to pressure. After these measurements, the signal, contraction ratio, speed and acceleration are saved in ASCII files.

These twenty sets of experiments are performed for five different mass values of the load. The aim of doing this step is to insert mass as a variable into the model.

Data Processing: The collected data is read in Matlab environment. In this process, the generated force and frictional force are calculated for contraction and relaxation of the muscle, separately. By finding the contact surface and the pressure, the frictional force coefficient is measured. The frictional force coefficient is modeled, and the pressure is modeled with respect to the response of the contraction ratio against the change in pressure.

4. METHOD

The proposed control method comprises two mathematical models; 1) describing frictional force coefficient in terms of electrical current speed and contraction ratio, 2) relating rubbertuator pressure-contraction ratio in terms of electrical current speed and load mass. In this chapter, the proposed mathematical models are described in detail.

4.1 FRICTIONAL FORCE COEFFICIENT MODEL

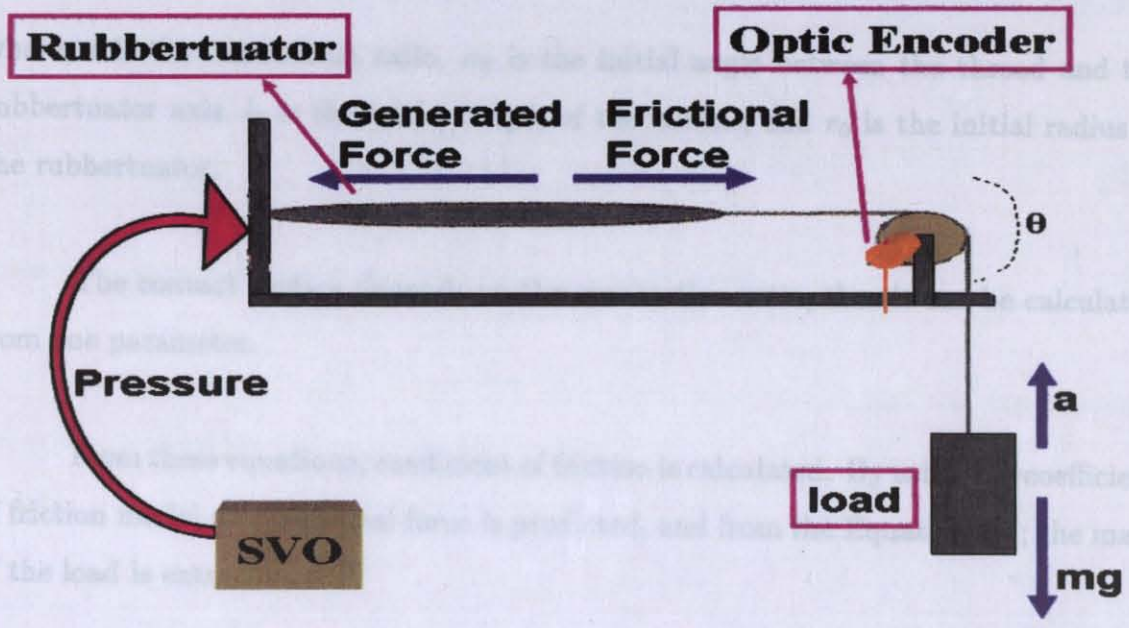

Figure 4.1 Forces generated by rubbertuator.

The directions of the generated forces on the system are seen in Figure 4.1. The generated force is calculated by using Equation 2.8. The frictional force is then calculated by Equation 4.1:

$$F_{friction} = F_{generated} - ma - mg \tag{4.1}$$

where, m is the mass of the load, a is the net acceleration and g is the gravitational

force. The frictional force is equal to the frictional force coefficient multiplied by the normal force on the muscle. The normal force is equal to the contact surface between the threads multiplied by the pressure.

$$F_{friction} = f S_{contact} P \tag{4.2}$$

where, f is the coefficient of friction, $S_{contact}$ is the area of the contact surface, P is pressure.

$$S_{contact} = \frac{2\pi r_0 l_0 \sin(\alpha_0)}{(1-\varepsilon)\sqrt{1-\cos\alpha_0(1-\varepsilon)^2}} \tag{4.3}$$

where, ε is the contraction ratio, α_0 is the initial angle between the thread and the rubbertuator axis, l_0 is the initial length of the muscle, and r_0 is the initial radius of the rubbertuator.

The contact surface depends on the contraction ratio, thus it can be calculated from one parameter.

From these equations, coefficient of friction is calculated. By using the coefficient of friction model, the frictional force is predicted, and from the Equation 4.1; the mass of the load is extracted.

The analysis of the data to model the coefficient of friction is done as follows: First a function is selected that may fit the data of coefficient of friction, then the data is fitted by this function for each electrical current speed and then the coefficients of the function are found. To find this relation, some commonly known functions are taken into consideration, such as Chi-square distribution, polynomial functions with high orders, exponential and logarithmic functions. All these functions except polynomial ones do not fit to the data. Polynomial function of fifth order or higher fits best, but their coefficients for different electrical current speeds do not provide satisfactory results. No relation could be found for the coefficients with different current speeds.

In addition, most of the curve can be fitted to any polynomial by increasing the order, so it is not useful to find the real relation between the data.

In Chi-square model, the relation between the coefficient of friction and contraction ratio is as in the following formula:

$$f = \frac{\varepsilon^{(\frac{v-2}{2})} exp^{(\frac{-\varepsilon}{2})}}{2^{(\frac{v}{2})}\Gamma(\frac{v}{2})} \tag{4.4}$$

where; f is the coefficient of friction, Γ is the Gamma function, and v is the degrees of freedom.

In fifth order polynomial model, the relation between the coefficient of friction and contraction ratio is as in the following formula:

$$f = p_0 + p_1\varepsilon + p_2\varepsilon^2 + p_3\varepsilon^3 + p_4\varepsilon^4 + p_5\varepsilon^5 \tag{4.5}$$

where; p_0, p_1, p_2, p_3, p_4, and p_5 are polynomial coefficients.

In Figures 4.2, 4.3, 4.4, 4.5, 4.6; the Chi-square model and the experimental data is compared for different current speeds.

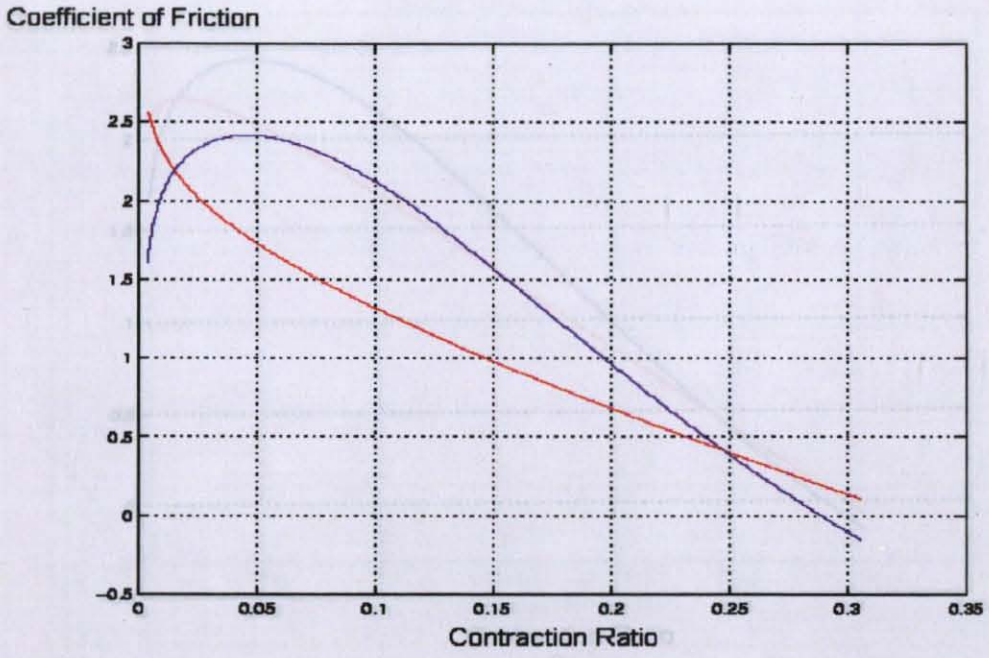

Figure 4.2 Chi-square Modeling: Coefficient of friction vs contraction ratio for 5.6 mA/sec current speed. Blue: experimental data, red: model's values.

Figure 4.3 Chi-square Modeling: Coefficient of friction vs contraction ratio for 6.7 mA/sec current speed. Blue: experimental data, red: model's values.

Figure 4.4 Chi-square Modeling: Coefficient of friction vs contraction ratio for 8.3 mA/sec current speed. Blue: experimental data, red: model's values.

Figure 4.5 Chi-square Modeling: Coefficient of friction vs contraction ratio for 11.1 mA/sec current speed. Blue: experimental data, red: model's values.

Figure 4.6 Chi-square Modeling: Coefficient of friction vs contraction ratio for 16.7 mA/sec current speed. Blue: experimental data, red: model's values.

In Figures 4.7, 4.8, 4.9, 4.10, 4.11; Fifth Order Polynomial Model and the experimental data is compared for different current speeds.

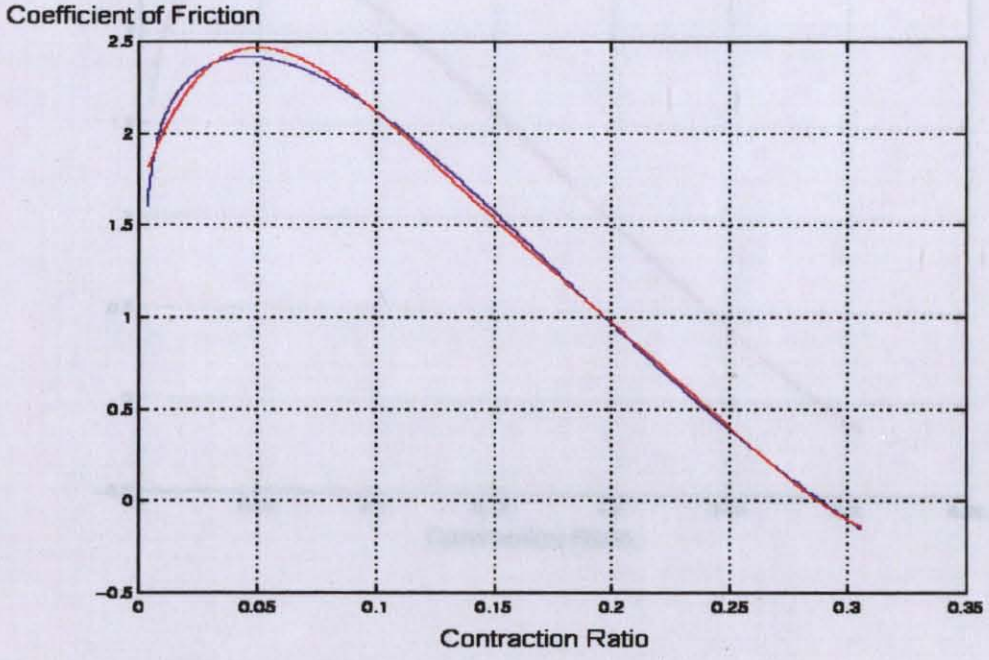

Figure 4.7 Fifth Order Polynomial Modeling: Coefficient of friction vs contraction ratio for 5.6 mA/sec current speed. Blue: experimental data, red: model's values.

Figure 4.8 Fifth Order Polynomial Modeling: Coefficient of friction vs contraction ratio for 6.7 mA/sec current speed. Blue: experimental data, red: model's values.

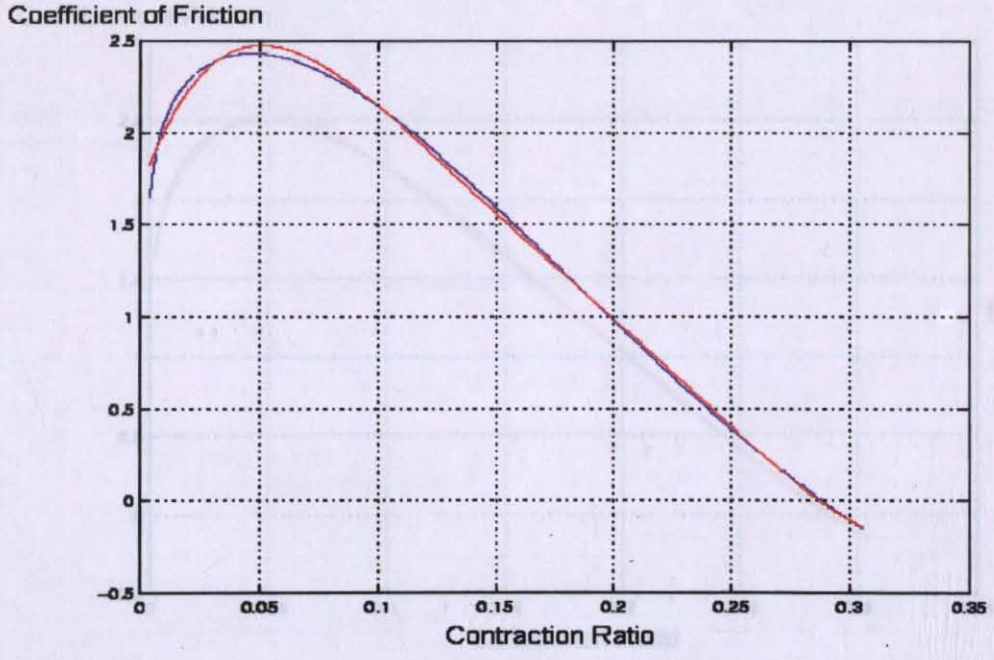

Figure 4.9 Fifth Order Polynomial Modeling: Coefficient of friction vs contraction ratio for 8.3 mA/sec current speed. Blue: experimental data, red: model's values.

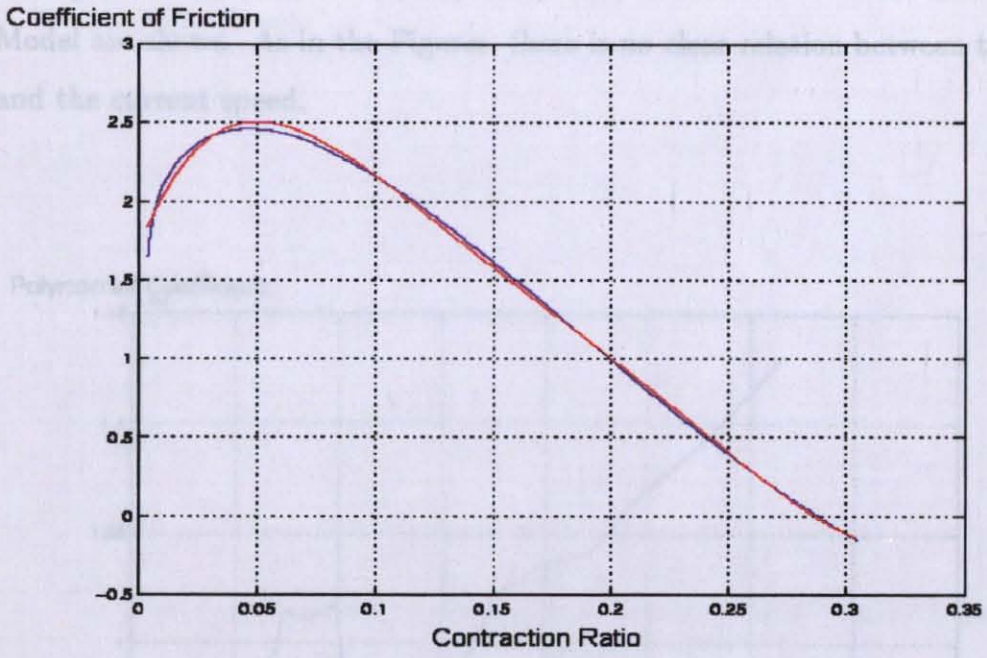

Figure 4.10 Fifth Order Polynomial Modeling: Coefficient of friction vs contraction ratio for 11.1 mA/sec current speed. Blue: experimental data, red: model's values.

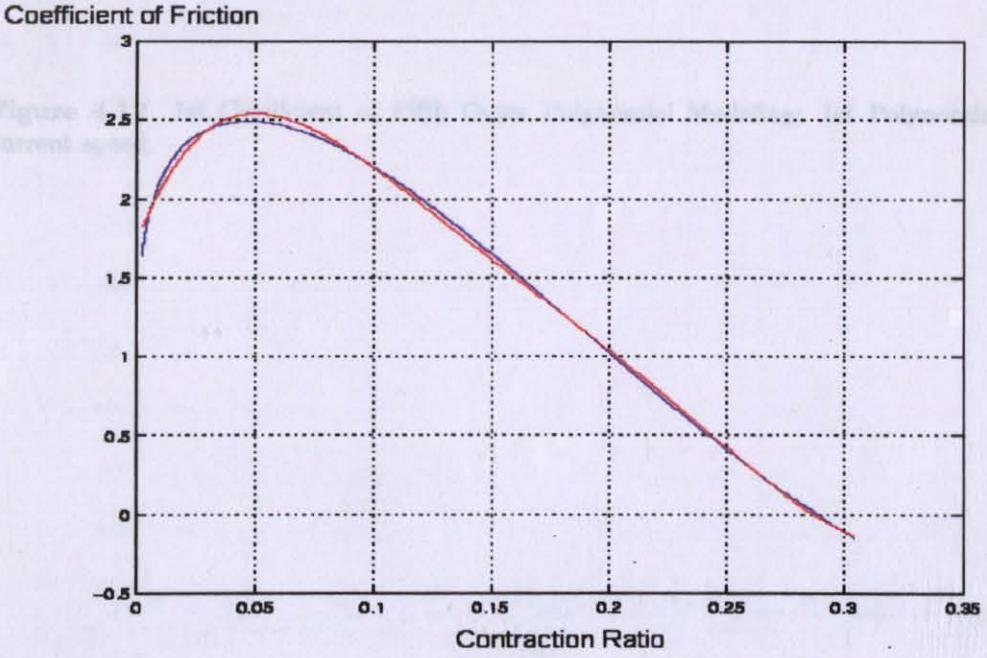

Figure 4.11 Fifth Order Polynomial Modeling: Coefficient of friction vs contraction ratio for 16.7 mA/sec current speed. Blue: experimental data, red: model's values.

In Figures 4.12, 4.13, 4.14, 4.15, 4.16, 4.17; coefficients of Fifth Order Polynomial Model are shown. As in the Figures, there is no clear relation between the coefficients and the current speed.

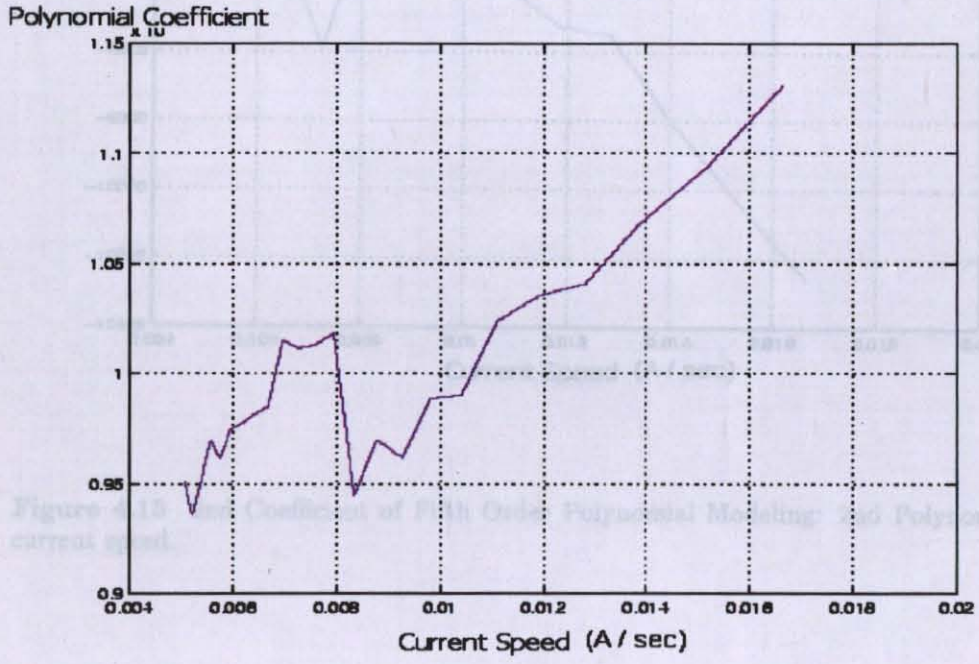

Figure 4.12 1st Coefficient of Fifth Order Polynomial Modeling: 1st Polynomial Coefficient vs current speed.

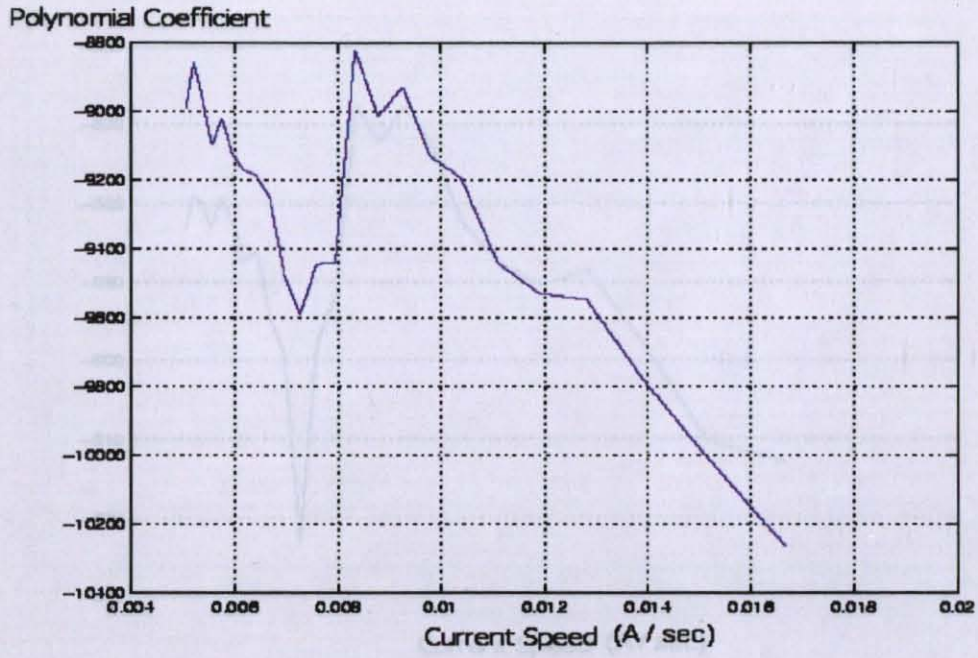

Figure 4.13 2nd Coefficient of Fifth Order Polynomial Modeling: 2nd Polynomial Coefficient vs current speed.

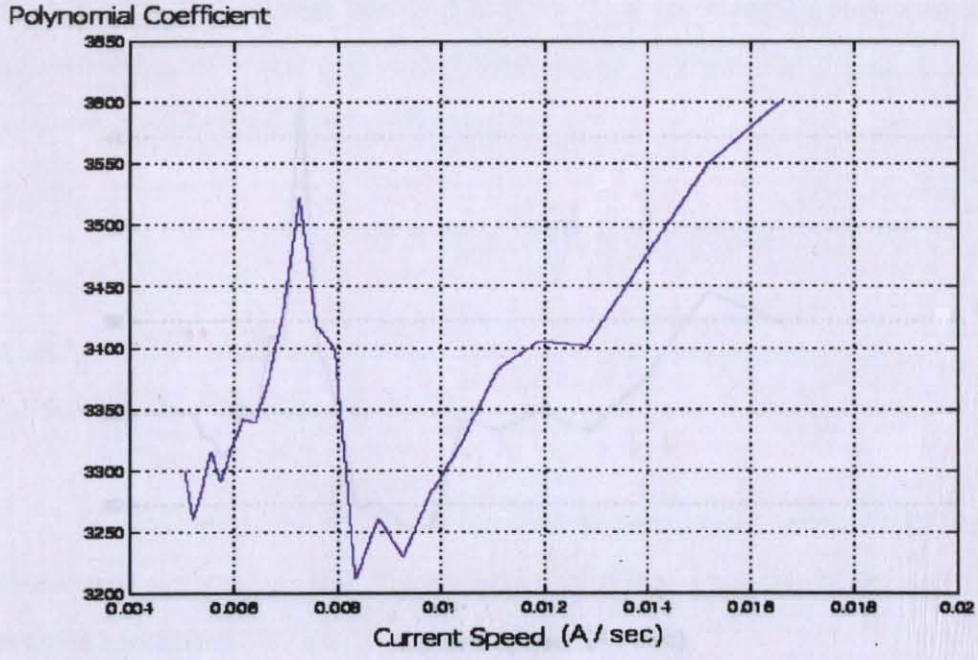

Figure 4.14 3rd Coefficient of Fifth Order Polynomial Modeling: 3rd Polynomial Coefficient vs current speed.

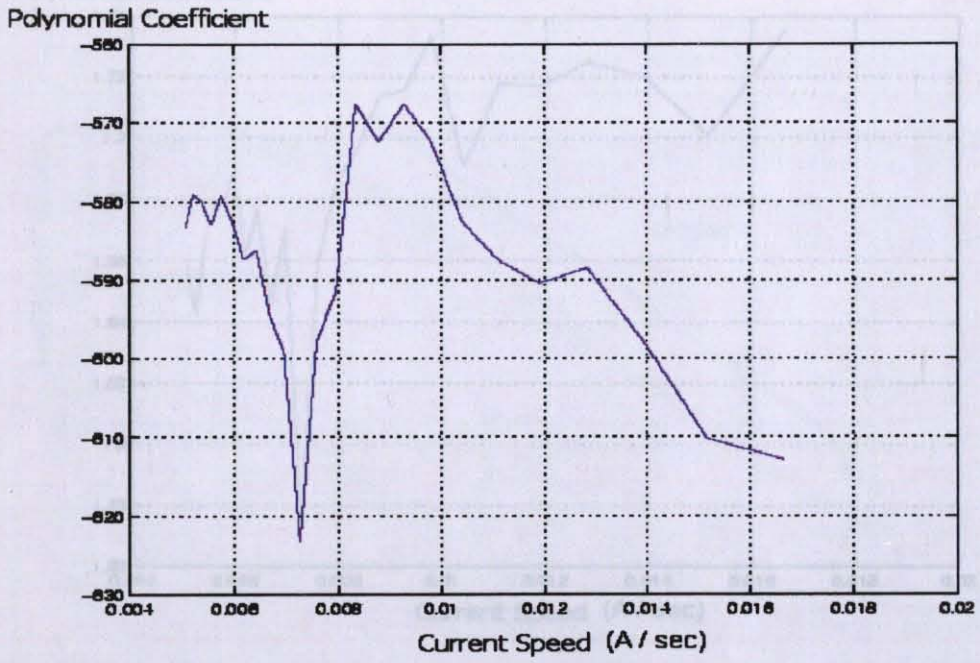

Figure 4.15 4th Coefficient of Fifth Order Polynomial Modeling: 4th Polynomial Coefficient vs current speed.

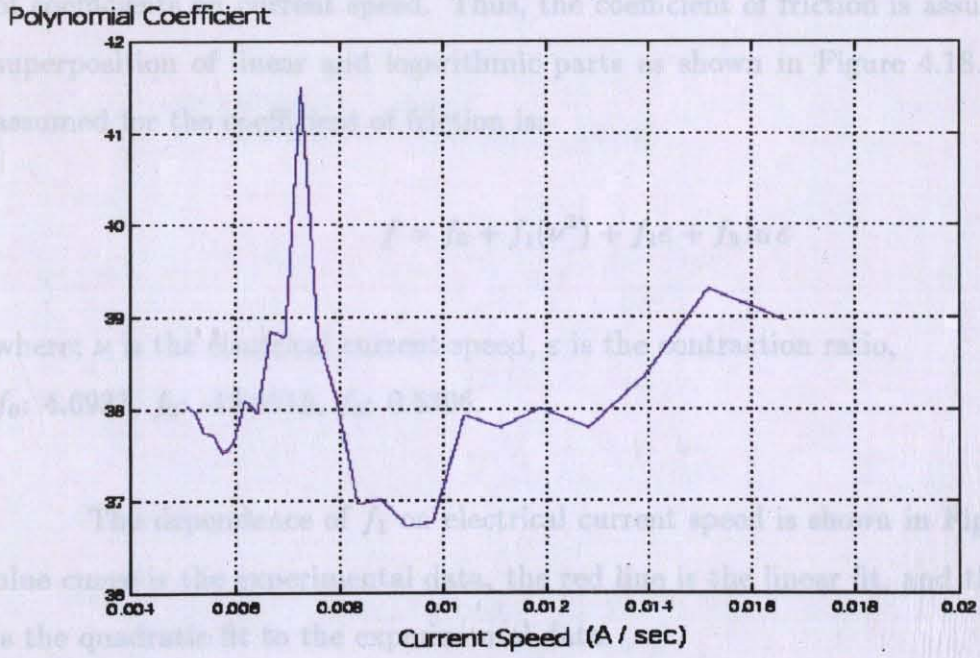

Figure 4.16 5th Coefficient of Fifth Order Polynomial Modeling: 5th Polynomial Coefficient vs current speed.

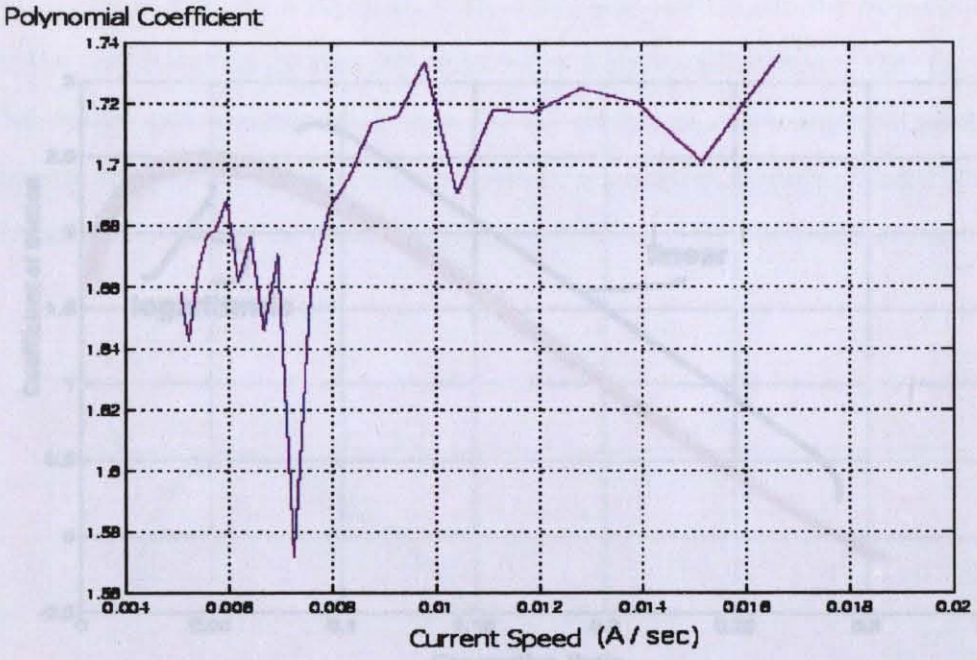

Figure 4.17 6th Coefficient of Fifth Order Polynomial Modeling: 6th Polynomial Coefficient vs current speed.

The Chi-square and Fifth Order Polynomial models fail to find the dependence of coefficients on current speed. Thus, the coefficient of friction is assumed to be the superposition of linear and logarithmic parts as shown in Figure 4.18. The formula assumed for the coefficient of friction is:

$$f = f_0 + f_1(\nu^2) + f_2\varepsilon + f_3 \ln \varepsilon \tag{4.6}$$

where; ν is the electrical current speed, ε is the contraction ratio,
f_0: 4.6937, f_2: -13.9715, f_3: 0.5306.

The dependence of f_1 on electrical current speed is shown in Figure 4.19. The blue curve is the experimental data, the red line is the linear fit, and the green curve is the quadratic fit to the experimental data.

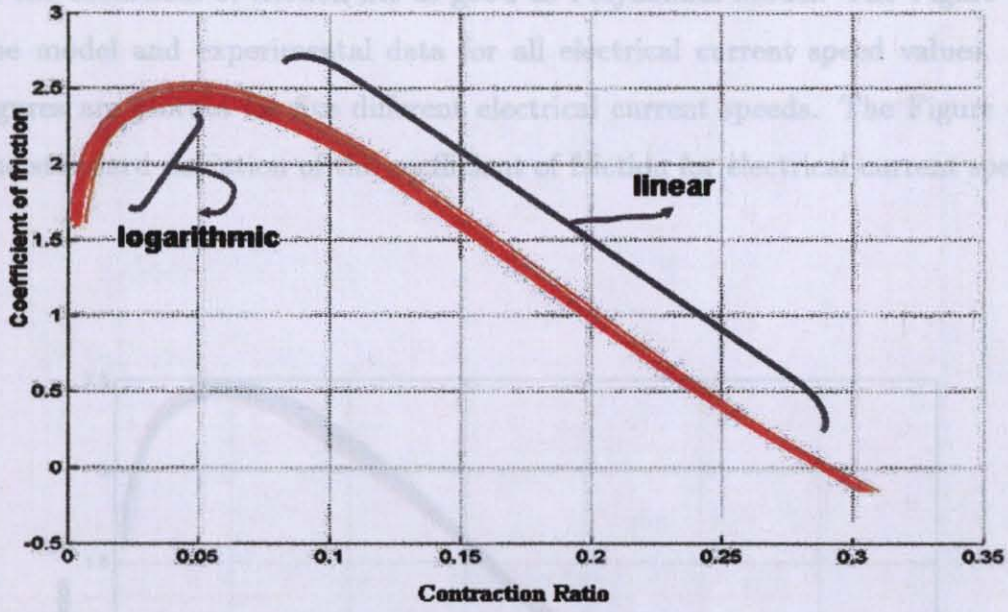

Figure 4.18 Superpositional modeling of the coefficient of friction with respect to contraction ratio.

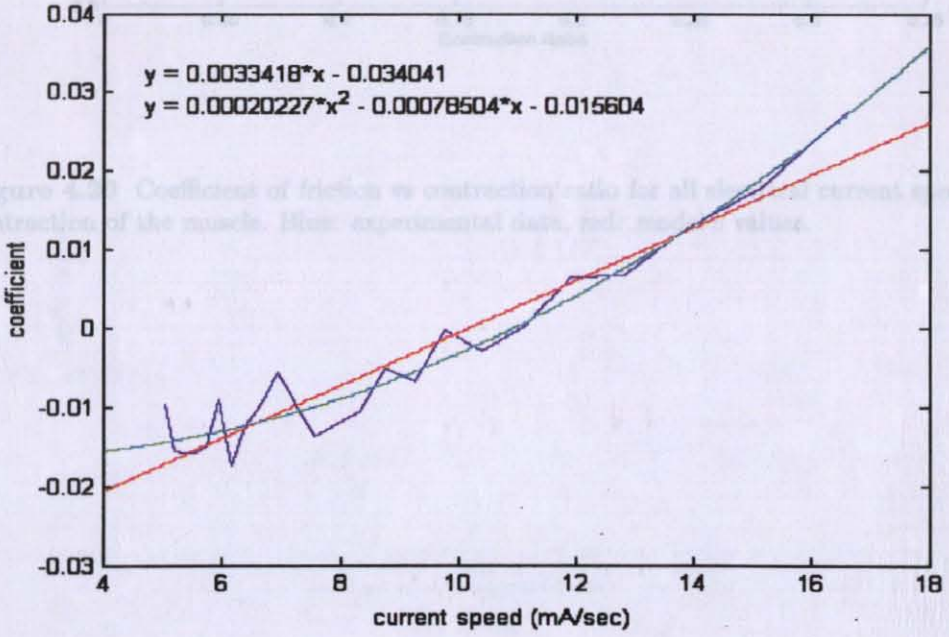

Figure 4.19 Dependence of $f_1(v^2)$ on current speed. Blue curve: experimental data, Red line: linear fit, and Green curve: quadratic fit to the experimental data.

As in Figures 4.20, 4.21, 4.22, 4.23, 4.24, and 4.25, the Superpositional Model of the coefficient of friction fits as good as Polynomial Model. The Figure 4.20 shows the model and experimental data for all electrical current speed values. The other figures are plotted for five different electrical current speeds. The Figure 4.26 shows the standard deviation of the coefficient of friction for electrical current speed values.

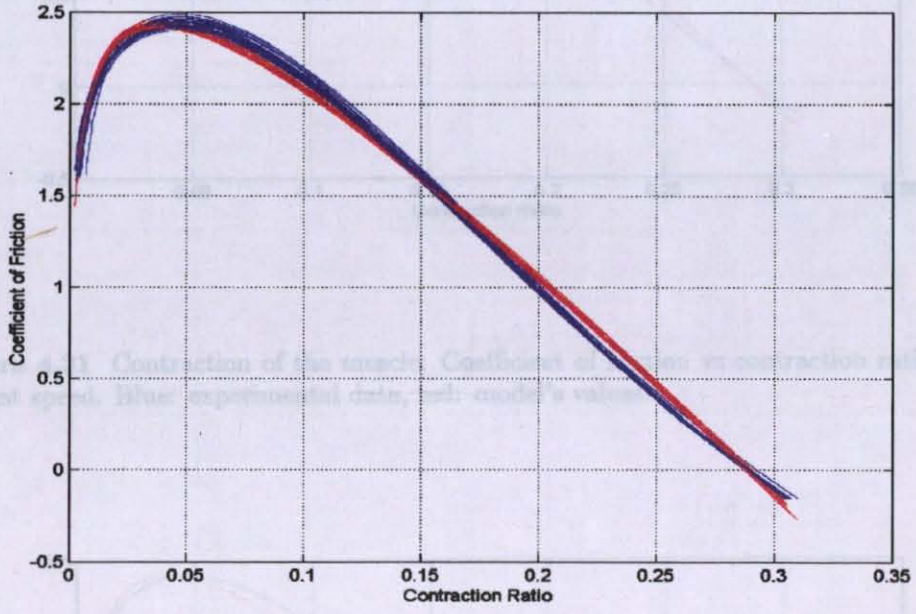

Figure 4.20 Coefficient of friction vs contraction ratio for all electrical current speed values for the contraction of the muscle. Blue: experimental data, red: model's values.

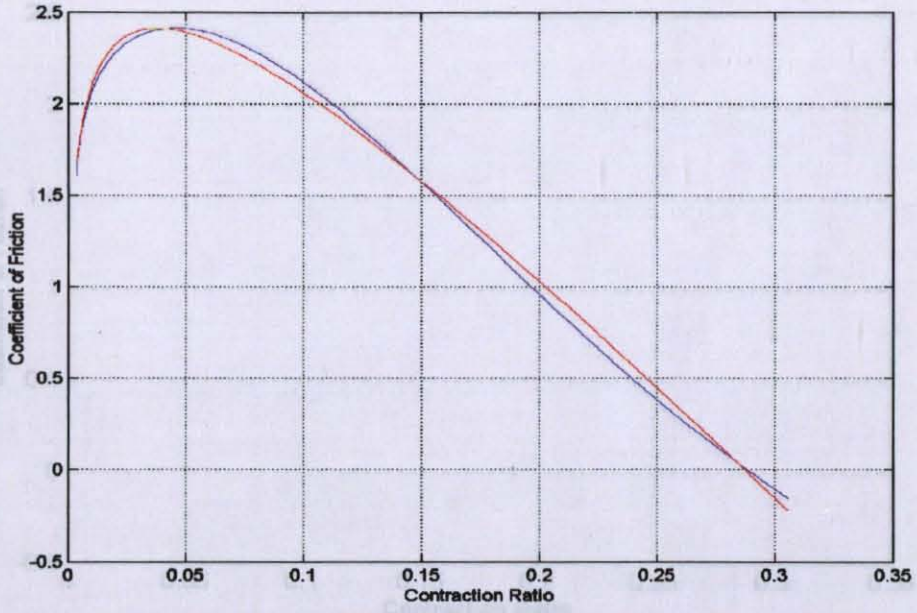

Figure 4.21 Contraction of the muscle: Coefficient of friction vs contraction ratio for 5.6 mA/sec current speed. Blue: experimental data, red: model's values.

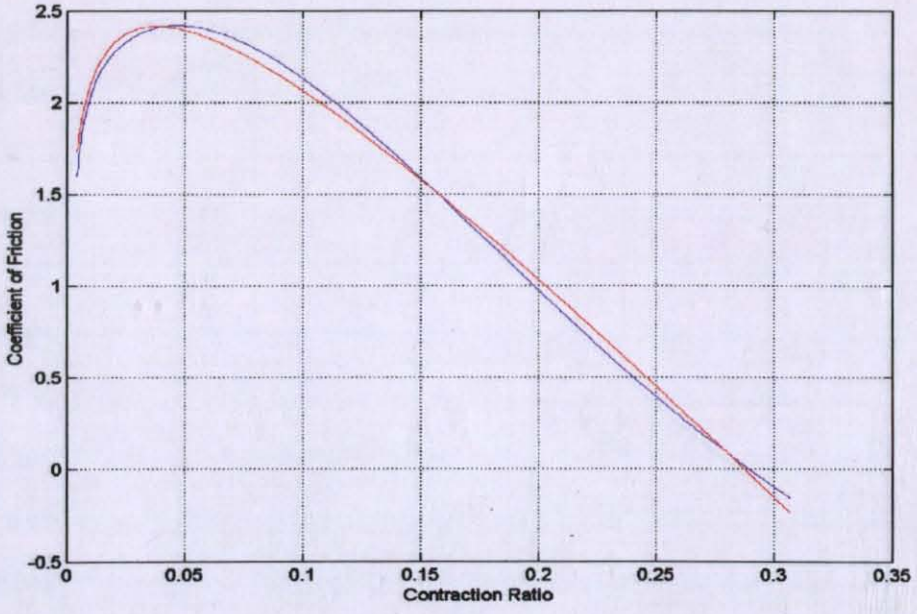

Figure 4.22 Contraction of the muscle: Coefficient of friction vs contraction ratio for 6.7 mA/sec current speed. Blue: experimental data, red: model's values.

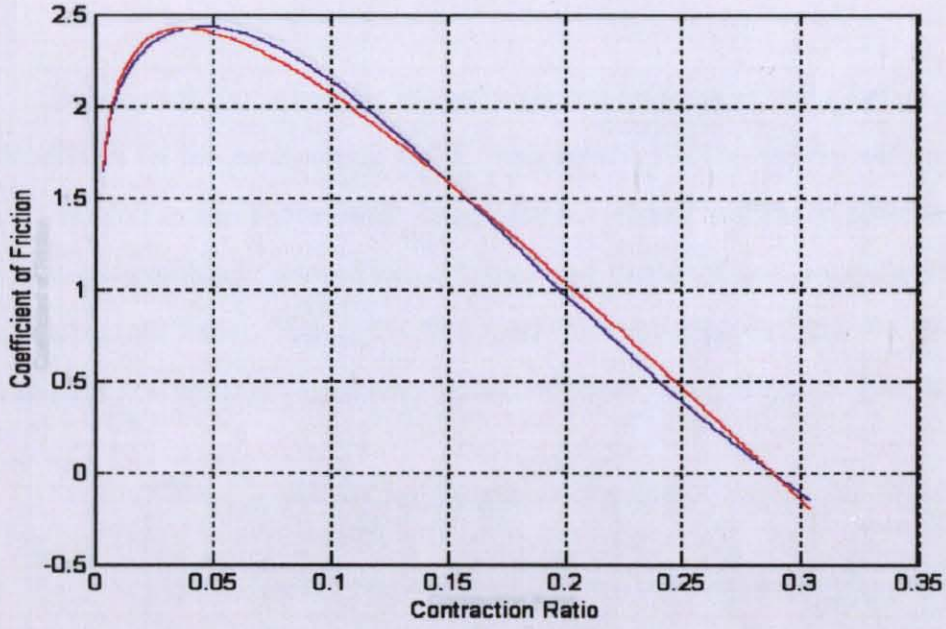

Figure 4.23 Contraction of the muscle: Coefficient of friction vs contraction ratio for 8.3 mA/sec current speed. Blue: experimental data, red: model's values.

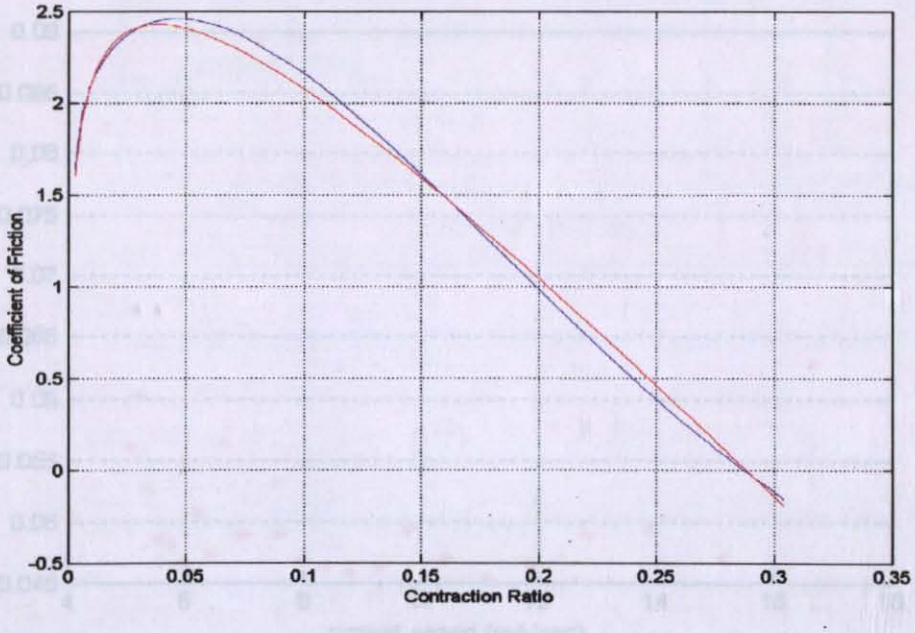

Figure 4.24 Contraction of the muscle: Coefficient of friction vs contraction ratio for 11.1 mA/sec current speed. Blue: experimental data, red: model's values.

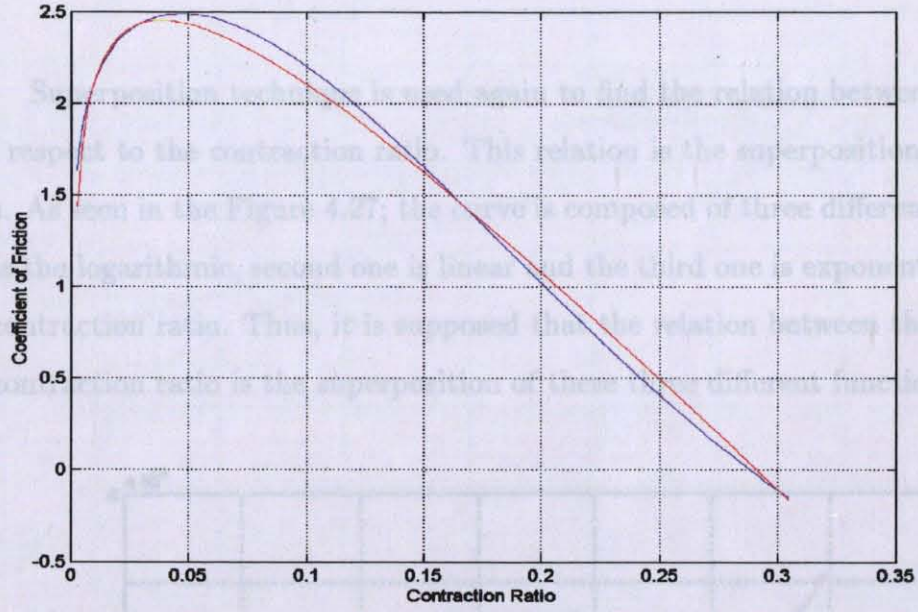

Figure 4.25 Contraction of the muscle: Coefficient of friction vs contraction ratio for 16.7 mA/sec current speed. Blue: experimental data, red: model's values.

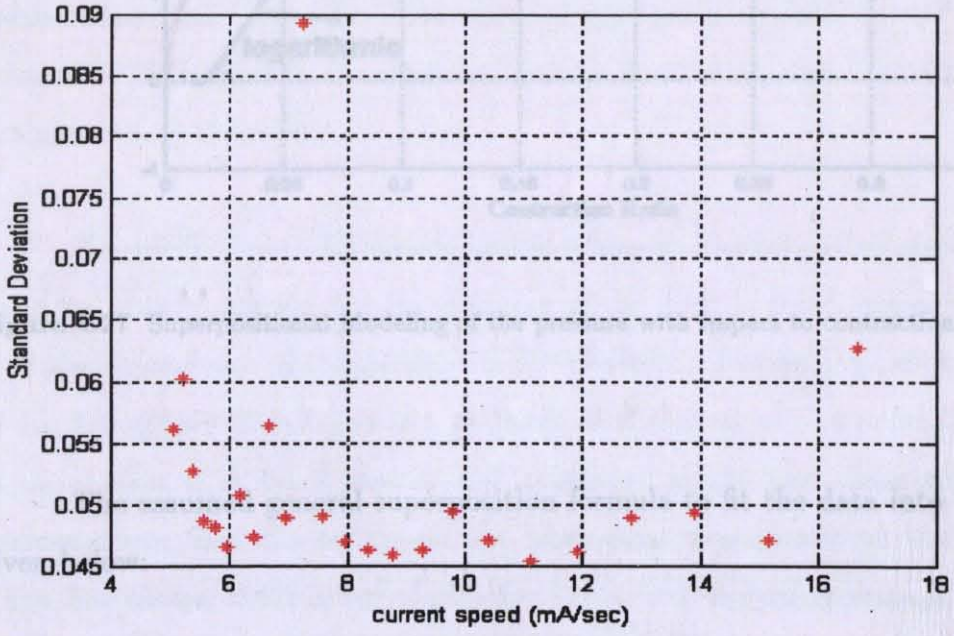

Figure 4.26 Standard Deviation in Coefficient of friction vs current speed.

4.2 PRESSURE-CONTRACTION RATIO MODEL

Superposition technique is used again to find the relation between the pressure with respect to the contraction ratio. This relation is the superposition of three functions. As seen in the Figure 4.27; the curve is composed of three different curves. First one is the logarithmic, second one is linear and the third one is exponential function of the contraction ratio. Thus, it is supposed that the relation between the pressure and the contraction ratio is the superposition of these three different functions.

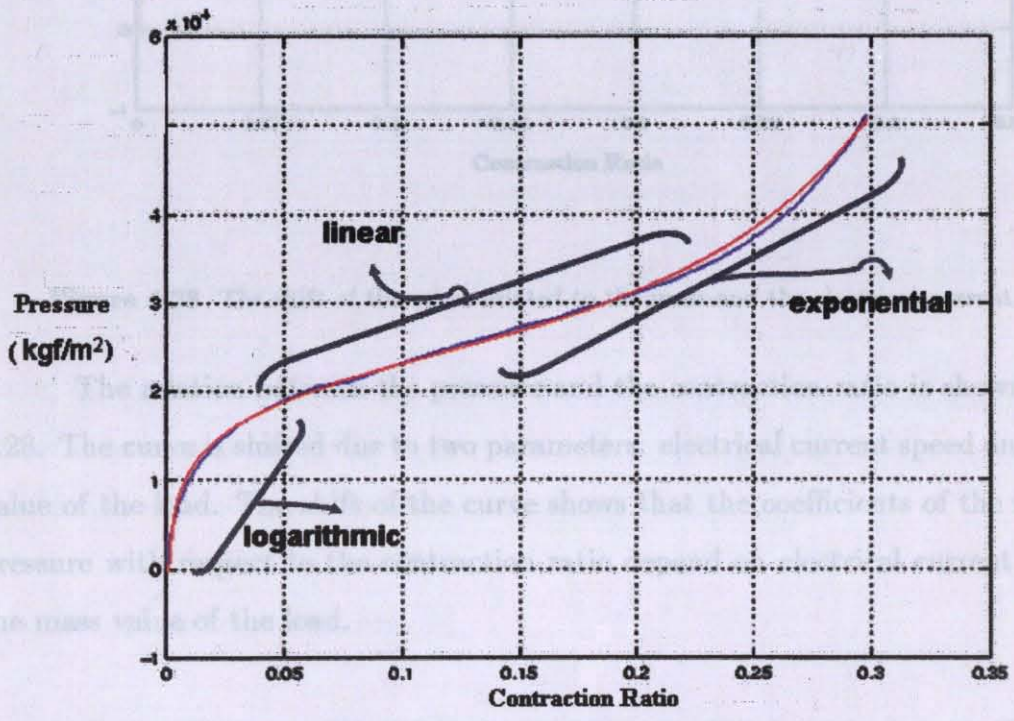

Figure 4.27 Superpositional Modeling of the pressure with respect to contraction ratio.

The assumed general superposition formula to fit the data into this curve is as given below:

$$P = a_0 + a_1\varepsilon + a_2 \exp(a_3\varepsilon) + a_4 \ln\varepsilon \tag{4.7}$$

where; P is pressure, ε is contraction ratio, $a_{0,1,..4}$ is the coefficients of the function.

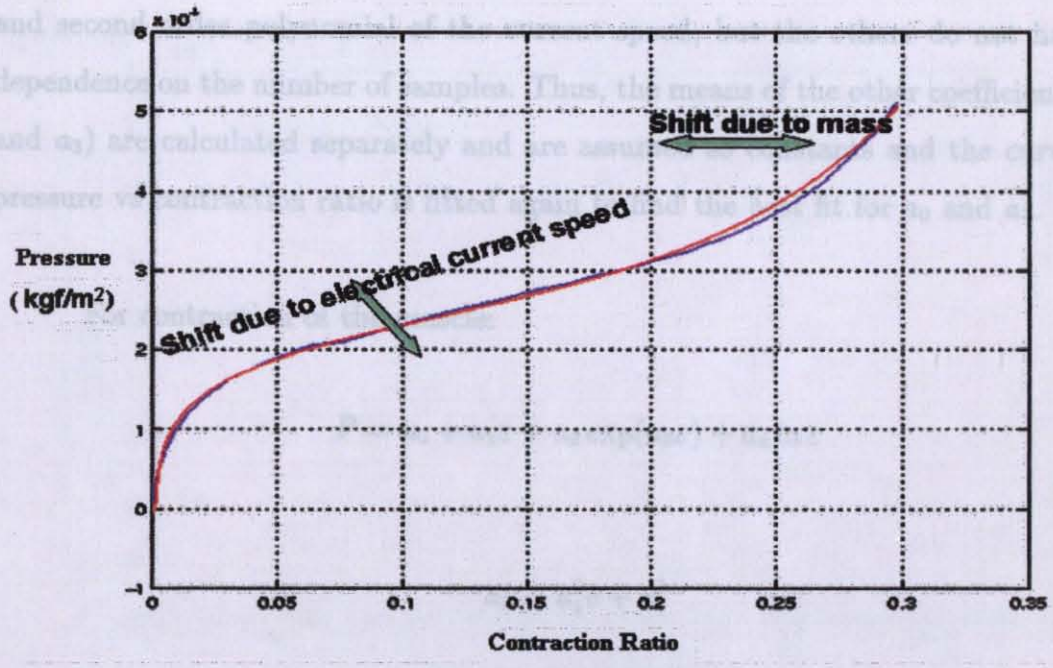

Figure 4.28 The shift of the curve related to the mass and the electrical current speed.

The relation between the pressure and the contraction ratio is shown in Figure 4.28. The curve is shifted due to two parameters: electrical current speed and the mass value of the load. The shift of the curve shows that the coefficients of the function of pressure with respect to the contraction ratio depend on electrical current speed and the mass value of the load.

The coefficients are found by curve-fitting in Matlab environment. For different electrical current speeds, the curve-fitting of the data to this function is performed so that the dependence of the coefficients to the electrical current speed is found. The set of coefficients are then fitted to a polynomial of first or second order. For contraction of the muscle, it is found that a_1 and a_2 depend on the first order polynomial of the current speed, but the others do not have clear dependence on the current speed. Thus, the means of the other coefficients (a_0, a_3 and a_4) are calculated separately and are assumed as constants and the curve of the pressure vs contraction ratio is fitted again to find the best fit for a_1 and a_2.

For relaxation of the muscle, it is found that a_0 and a_4 depend on the first and second order polynomial of the current speed, but the others do not have clear dependence on the number of samples. Thus, the means of the other coefficients (a_1, a_2 and a_3) are calculated separately and are assumed as constants and the curve of the pressure vs contraction ratio is fitted again to find the best fit for a_0 and a_4.

For contraction of the muscle:

$$P = a_0 + a_1\varepsilon + a_2 \exp(a_3\varepsilon) + a_4 \ln \varepsilon \tag{4.8}$$

$$a_1 = a_1^0 v + a_1^1 \tag{4.9}$$

$$a_2 = a_2^0 v + a_2^1 \tag{4.10}$$

where; a_0, a_3, and a_4 do not depend on the current speed. a_1 and a_2 depend on the electrical current as shown in Figure 4.29 and 4.30. a_1^0, a_1^1, a_2^0, a_2^1 are constants and depend only on the mass, and ν is the electrical current speed.

For relaxation of the muscle:

$$P = b_0 + b_1\varepsilon + b_2 \exp(b_3\varepsilon) + b_4 \ln \varepsilon \tag{4.11}$$

$$b_0 = b_0^0 v + b_0^1 \tag{4.12}$$

$$b_4 = b_4^0 v^2 + b_4^1 v + b_4^2 \tag{4.13}$$

where; b_1, b_2, and b_3 do not depend on the current speed. b_0 and b_4 depend on the electrical current as shown in Figure 4.31 and 4.32. b_0^0, b_0^1, b_4^0, b_4^1, b_4^2 are constants and depend only on the mass.

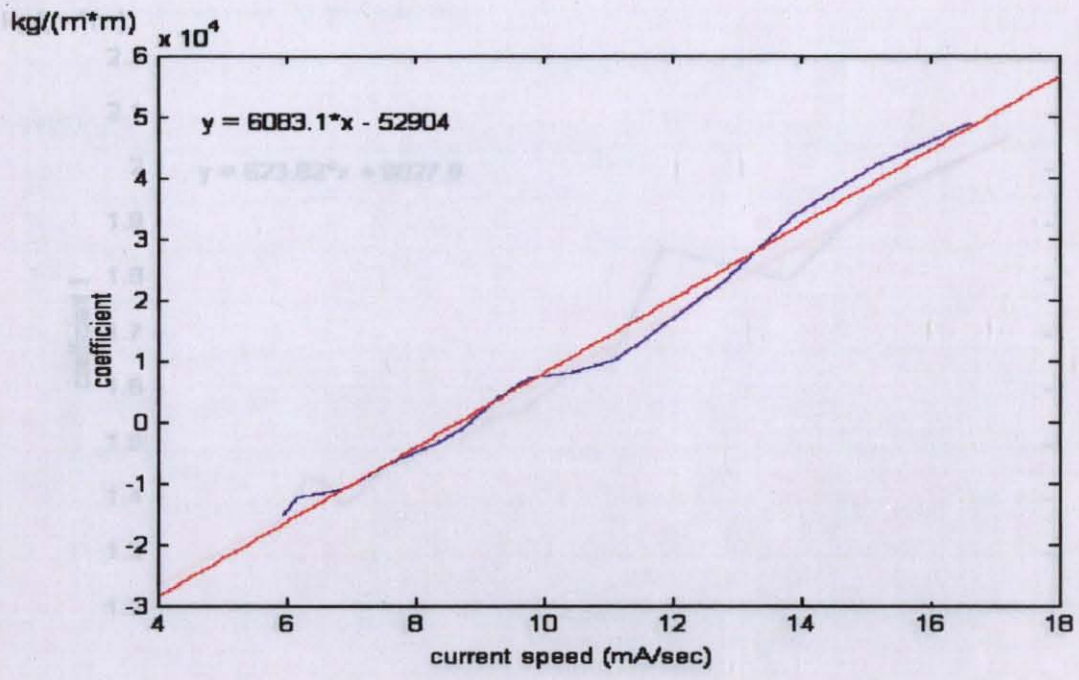

Figure 4.29 a_1 with respect to current speed for 11.1380 kg mass.

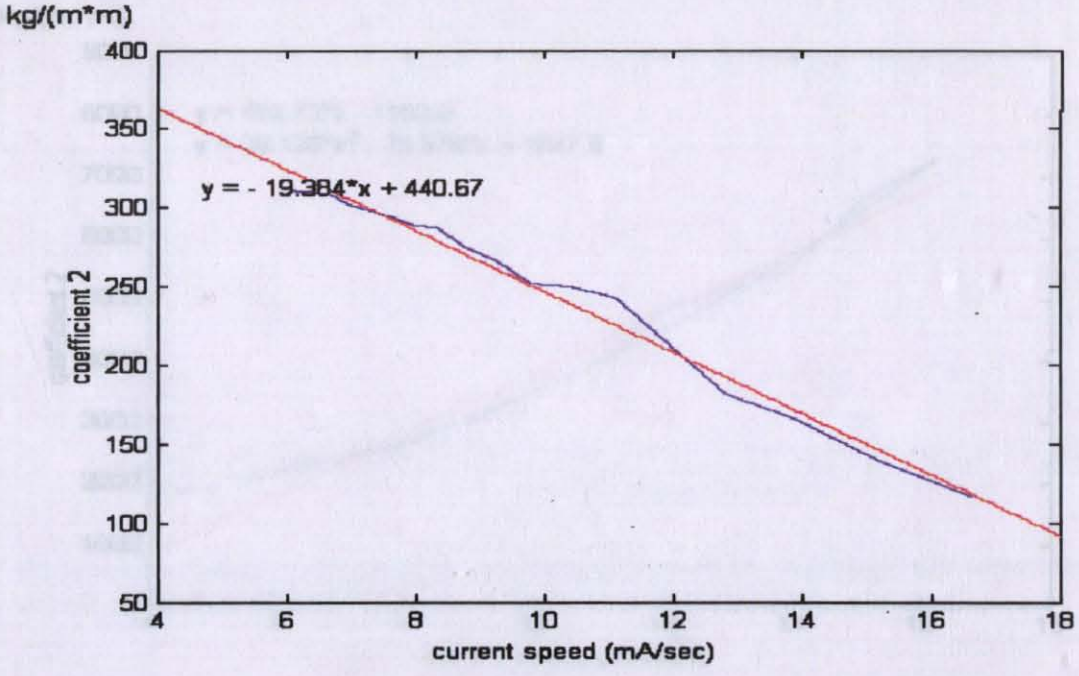

Figure 4.30 a_2 with respect to current speed for 11.1380 kg mass.

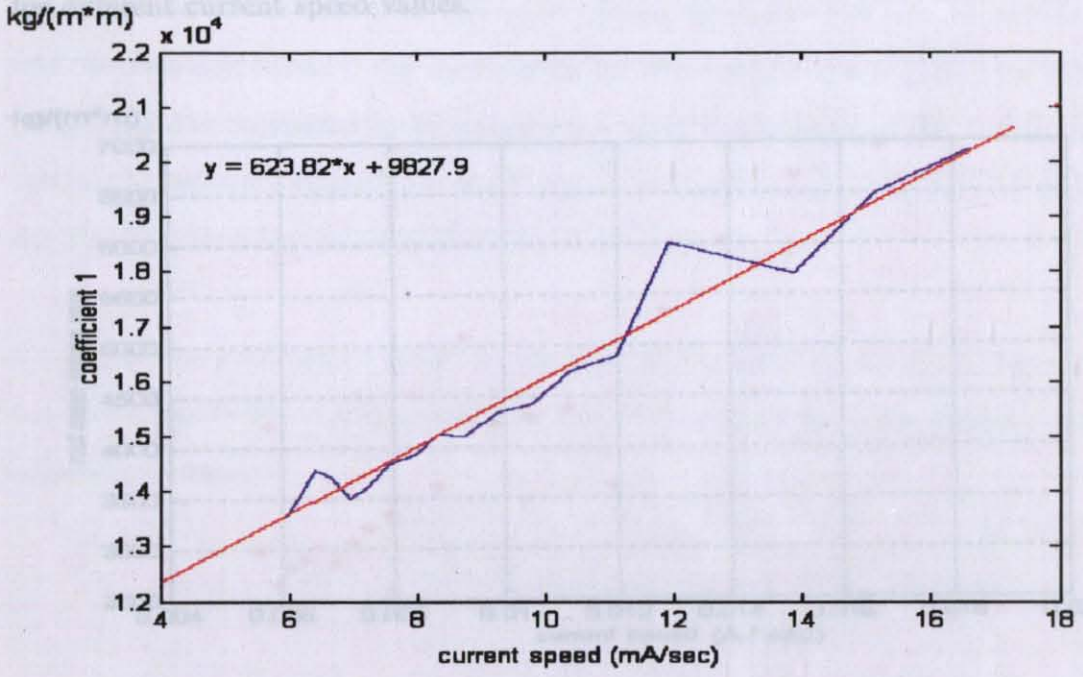

Figure 4.31 b_0 with respect to current speed for 11.1380 kg mass.

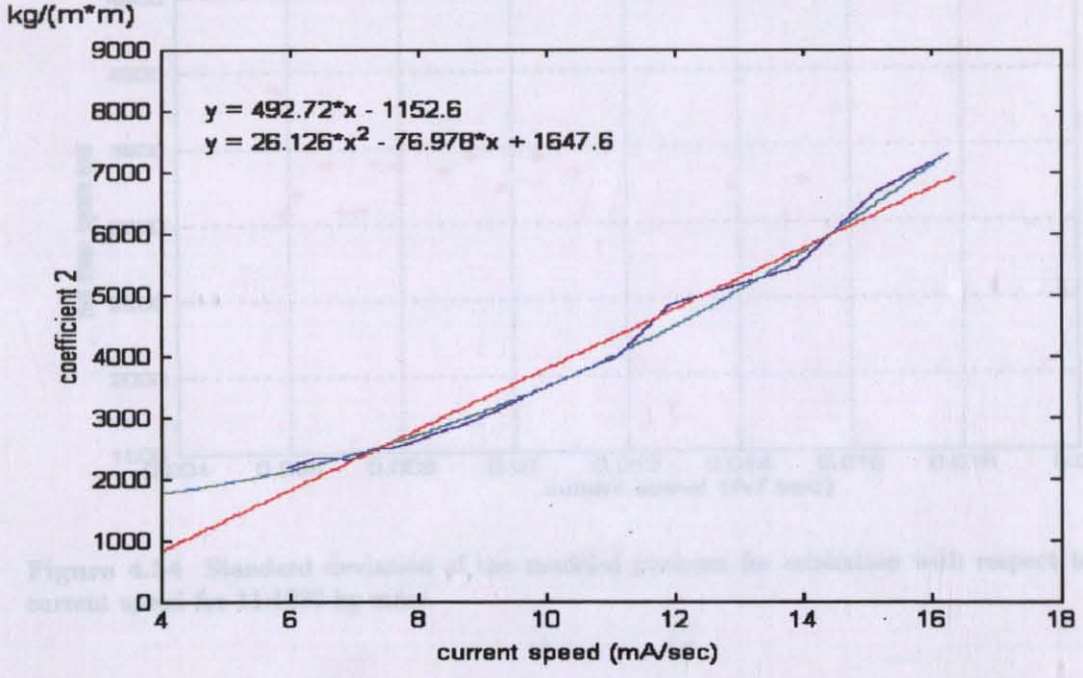

Figure 4.32 b_4 with respect to current speed for 11.1380 kg mass.

The Figures 4.33 and 4.34 show the standard deviation of the modeled pressure for different current speed values.

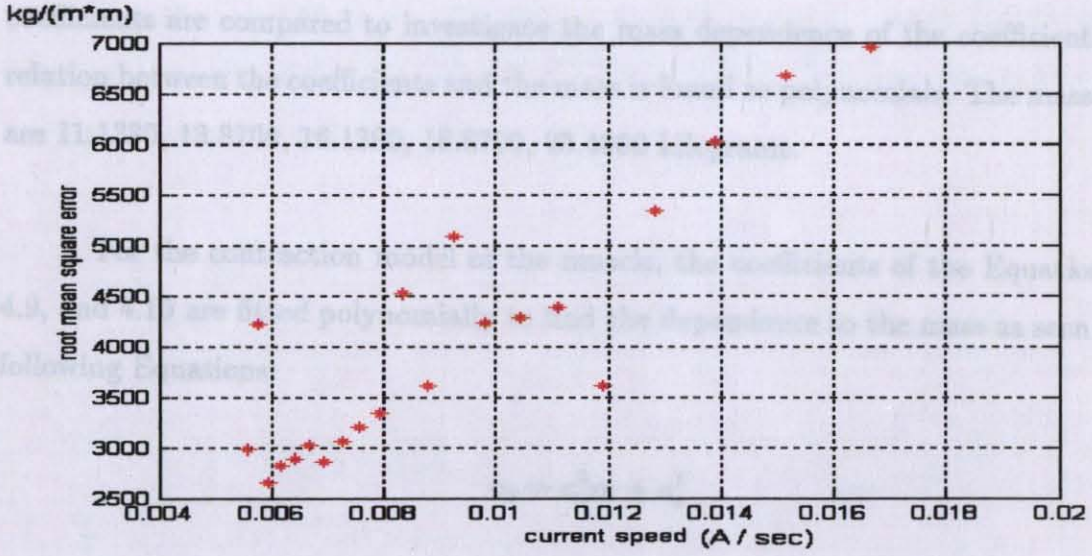

Figure 4.33 Standard deviation of the modeled pressure for contraction with respect to electrical current speed for 11.1380 kg mass.

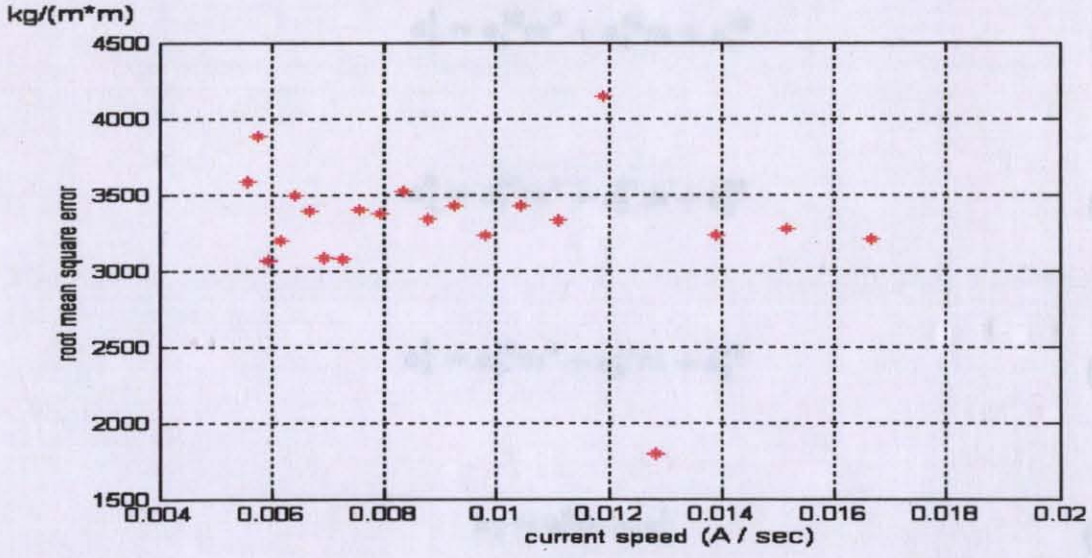

Figure 4.34 Standard deviation of the modeled pressure for relaxation with respect to electrical current speed for 11.1380 kg mass.

The set of calculations for 20 different current speeds are carried out 5 times for 5 different mass values of the load. Thus, there are 100 sets of calculations to find the relation between the coefficients and the current speed and mass value. The coefficients are compared to investigate the mass dependence of the coefficients. The relation between the coefficients and the mass is found as polynomials. The mass values are 11.1380, 13.8700, 16.1380, 18.8700, 23.4060 kilograms.

For the contraction model of the muscle, the coefficients of the Equations 4.8, 4.9, and 4.10 are fitted polynomially to find the dependence to the mass as seen in the following Equations:

$$a_0 = a_0^0 m + a_o^1 \tag{4.14}$$

$$a_1^0 = a_1^{00} m^3 + a_1^{01} m^2 + a_1^{02} m + a_1^{03} \tag{4.15}$$

$$a_1^1 = a_1^{10} m^2 + a_1^{11} m + a_1^{12} \tag{4.16}$$

$$a_2^0 = a_2^{00} m^2 + a_2^{01} m + a_2^{02} \tag{4.17}$$

$$a_2^1 = a_2^{10} m^2 + a_2^{11} m + a_2^{12} \tag{4.18}$$

$$a_3 = a_3^0 m + a_3^1 \tag{4.19}$$

$$a_4 = a_4^0 m + a_4^1 \tag{4.20}$$

where; m is the mass of the load, $a_0^0, a_0^1, a_1^{00}, a_1^{01}, a_1^{02}, a_1^{10}, a_1^{11}, a_1^{12}, a_2^{00}, a_2^{01}, a_2^{02}, a_2^{10}$, a_2^{11}, a_2^{12}, a_3^0, a_3^1, a_4^0, and a_4^1 are constants of the polynomials. The subscripts show the

main number of the coefficients. The coefficients having one superscript are the sub-coefficients of the main coefficients. The coefficients having two superscripts are the sub-coefficients of the sub-coefficients. The coefficients $a_0, a_1^0, a_1^1, a_2^0, a_2^1, a_3$, and a_4 are plotted in Figures 4.35, 4.36, 4.37, 4.38, 4.39, 4.40, and 4.41. As in the Figures; the coefficients are fitted linearly or quadratically in Matlab. The functions in the Figures are the functions of fitting curves.

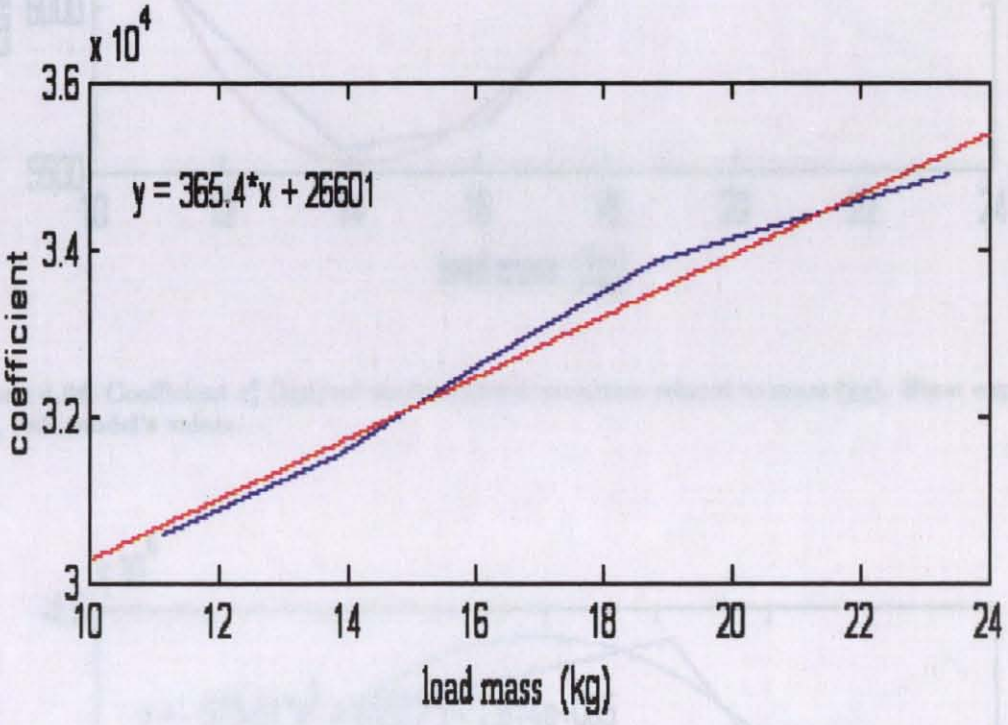

Figure 4.35 Coefficient a_0 (kgf/m^2) for contraction related to mass (kg). Blue: experimental data, red: model's values.

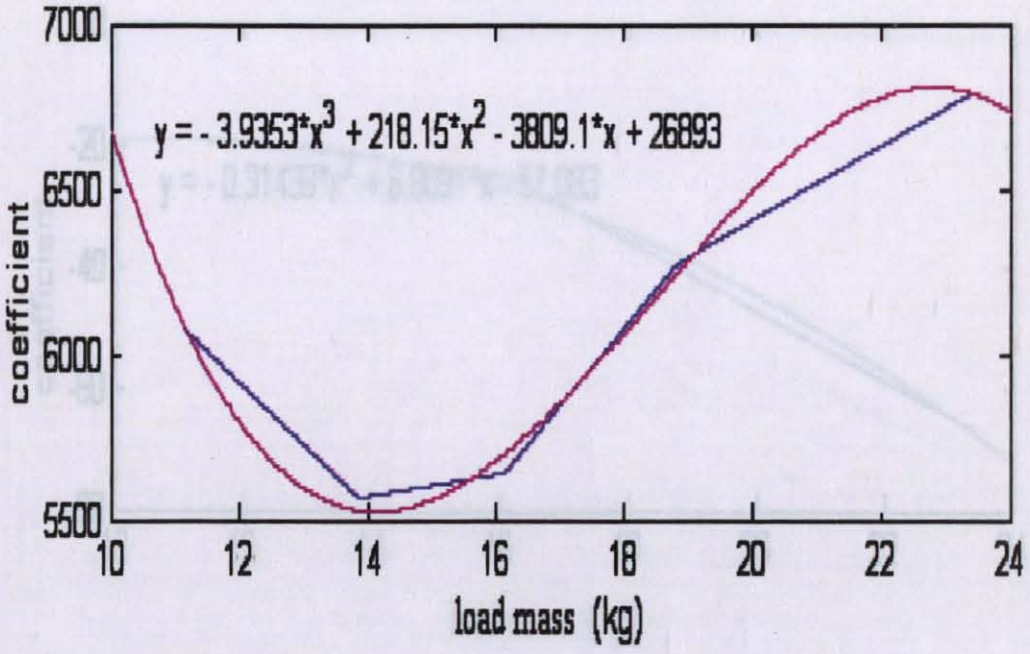

Figure 4.36 Coefficient a_1^0 (kgf/m^2 sec/mA) for contraction related to mass (kg). Blue: experimental data, red: model's values.

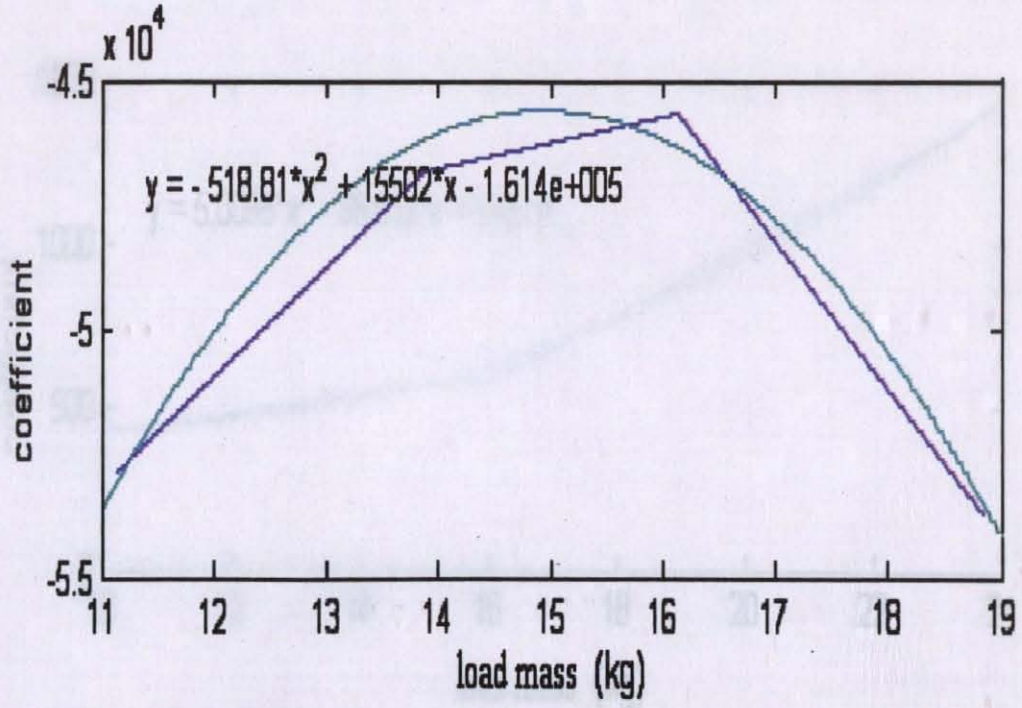

Figure 4.37 Coefficient a_1^1 (kgf/m^2) for contraction related to mass (kg). Blue: experimental data, green: model's values.

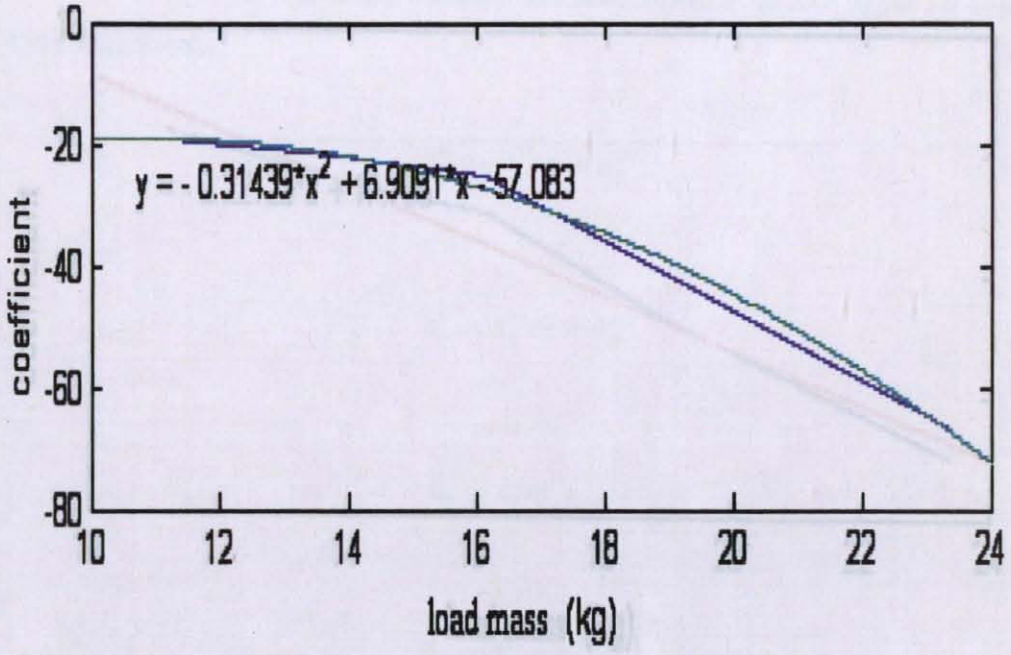

Figure 4.38 Coefficient a_2^0 (kgf/m^2 sec/mA) for contraction related to mass (kg). Blue: experimental data, green: model's values.

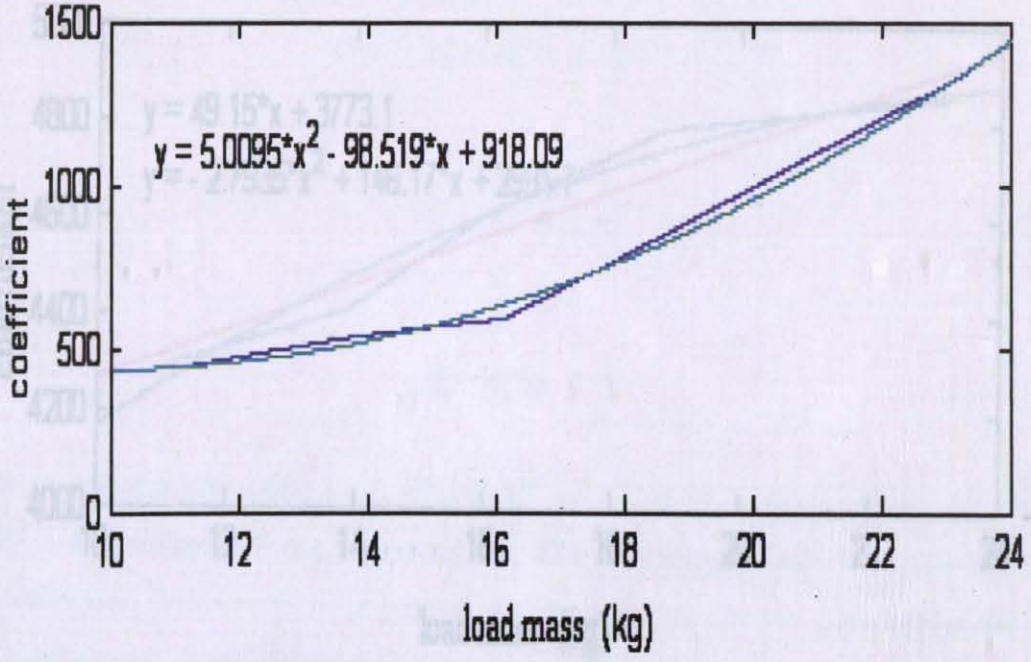

Figure 4.39 Coefficient a_2^1 (kgf/m^2) for contraction related to mass (kg). Blue: experimental data, green: model's values.

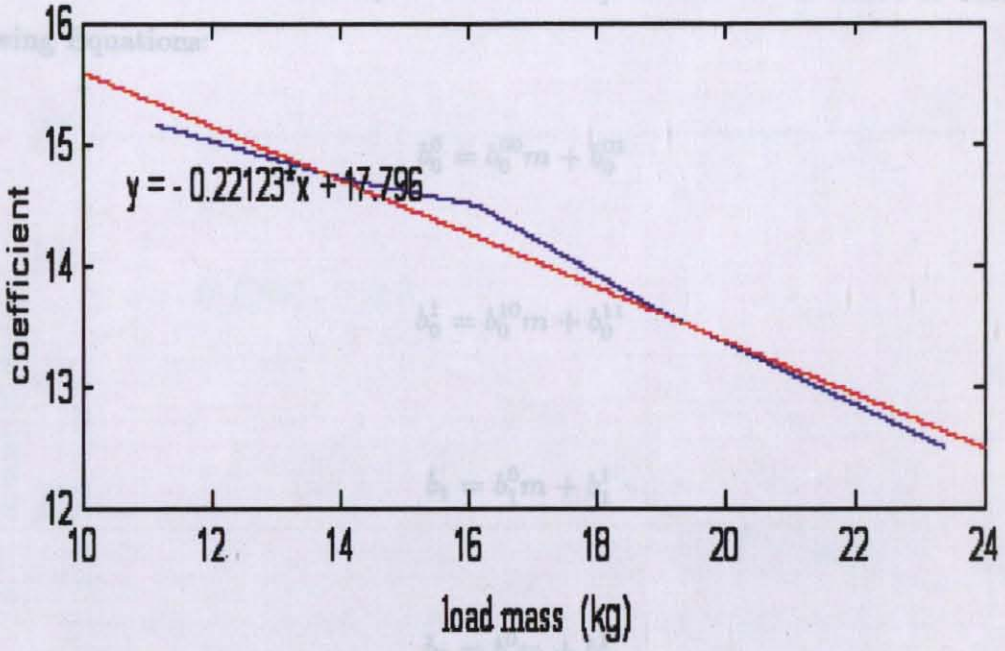

Figure 4.40 Coefficient a_3 (kgf/m^2) for contraction related to mass (kg). Blue: experimental data, red: model's values.

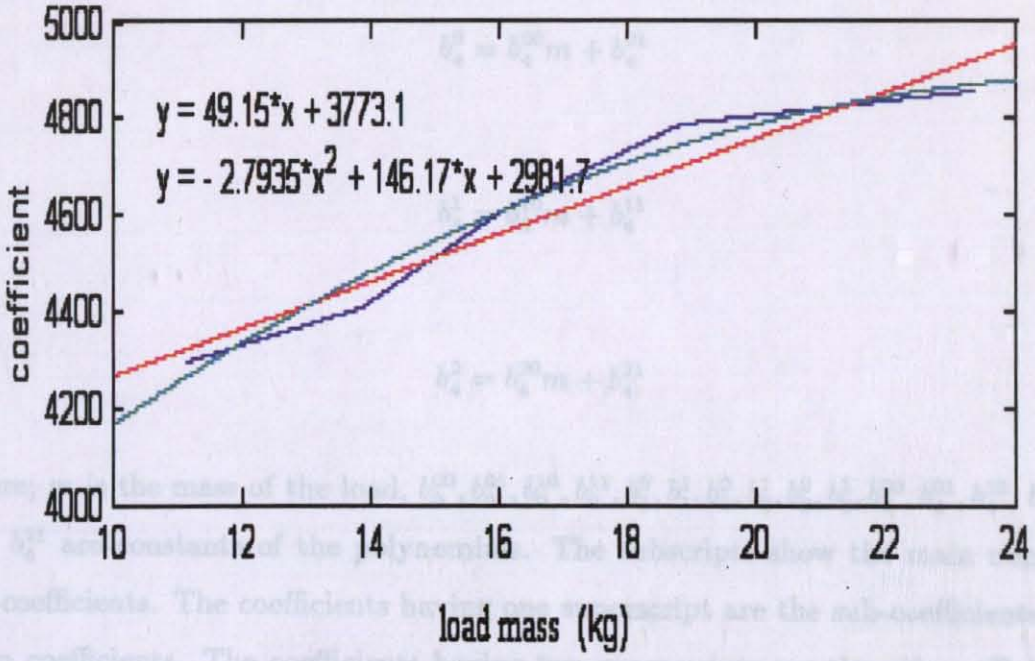

Figure 4.41 Coefficient a_4 (kgf/m^2) for contraction related to mass (kg). Blue: experimental data, red: model's linear values, green: model's quadratic values. Linear values are used in model

For the relaxation model of the muscle, the coefficients of the Equations 4.11, 4.12, and 4.13 are fitted linearly to find the dependence to the mass as seen in the following Equations:

$$b_0^0 = b_0^{00}m + b_0^{01} \tag{4.21}$$

$$b_0^1 = b_0^{10}m + b_0^{11} \tag{4.22}$$

$$b_1 = b_1^0 m + b_1^1 \tag{4.23}$$

$$b_2 = b_2^0 m + b_2^1 \tag{4.24}$$

$$b_3 = b_3^0 m + b_3^1 \tag{4.25}$$

$$b_4^0 = b_4^{00}m + b_4^{01} \tag{4.26}$$

$$b_4^1 = b_4^{10}m + b_4^{11} \tag{4.27}$$

$$b_4^2 = b_4^{20}m + b_4^{21} \tag{4.28}$$

where; m is the mass of the load, $b_0^{00}, b_0^{01}, b_0^{10}, b_0^{11}, b_1^0, b_1^1, b_2^0, b_2^1, b_3^0, b_3^1, b_4^{00}, b_4^{01}, b_4^{10}, b_4^{11}, b_4^{20}$, and b_4^{21} are constants of the polynomials. The subscripts show the main number of the coefficients. The coefficients having one superscript are the sub-coefficients of the main coefficients. The coefficients having two superscripts are the sub-coefficients of the sub-coefficients. The coefficients $b_0^0, b_0^1, b_1, b_2, b_3, b_4^0, b_4^1$, and b_4^2 are plotted in Figures 4.42, 4.43, 4.44, 4.45, 4.46, 4.47, 4.48, and 4.49. As in the Figures; the coefficients

are fitted linearly or quadratically in Matlab. The functions in the Figures are the functions of fitting curves.

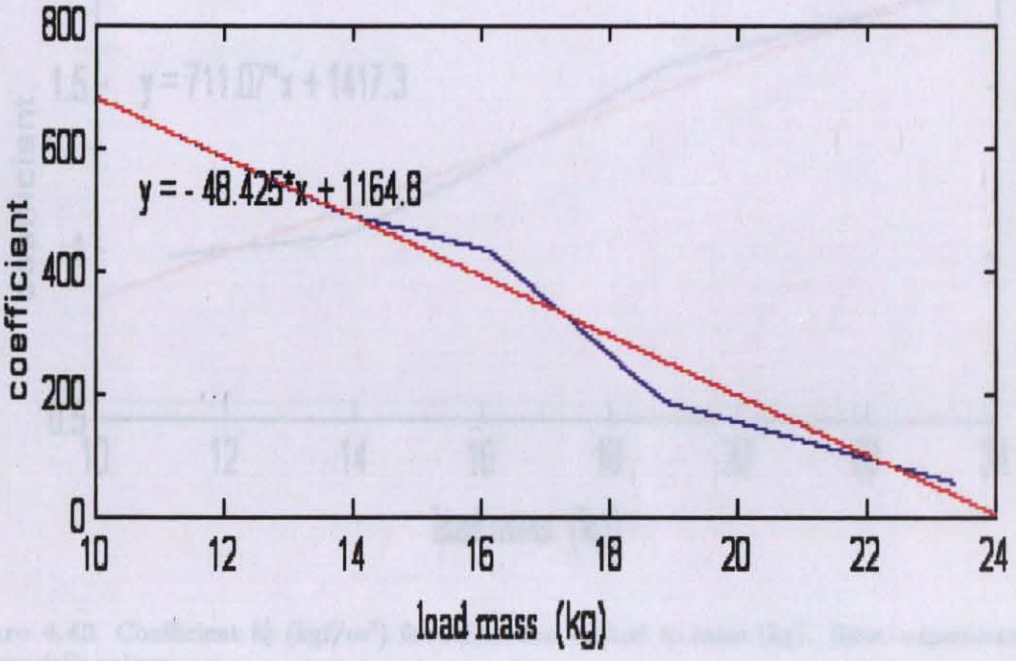

Figure 4.42 Coefficient b_0^0 (kgf/m^2 sec/mA) for relaxation related to mass (kg). Blue: experimental data, red: model's values.

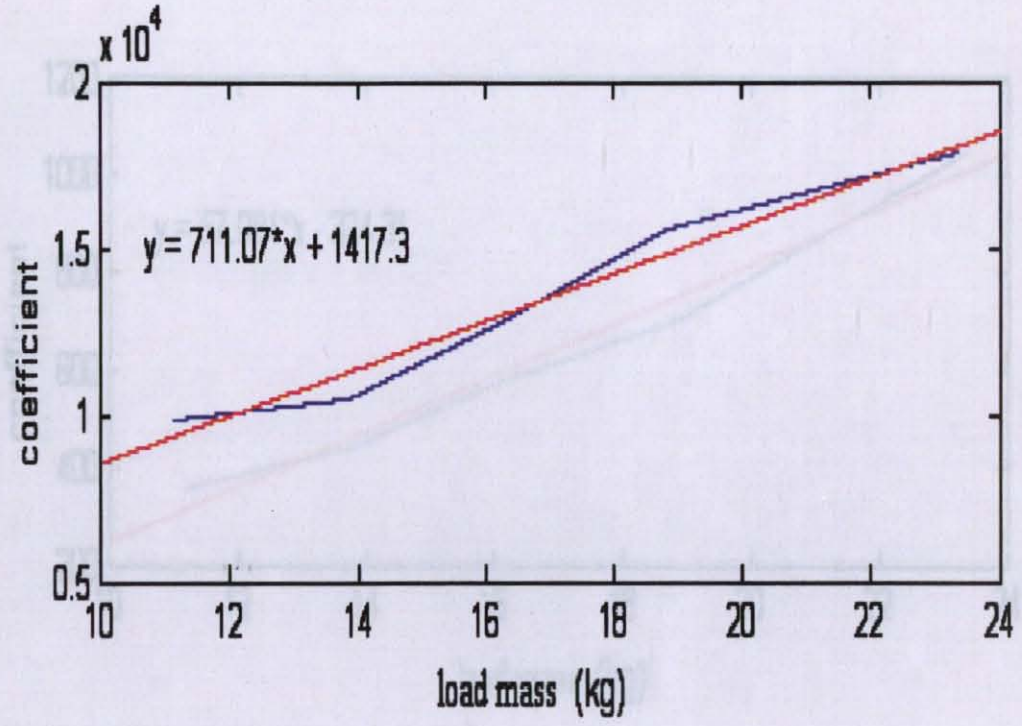

Figure 4.43 Coefficient b_0^1 (kgf/m^2) for relaxation related to mass (kg). Blue: experimental data, red: model's values.

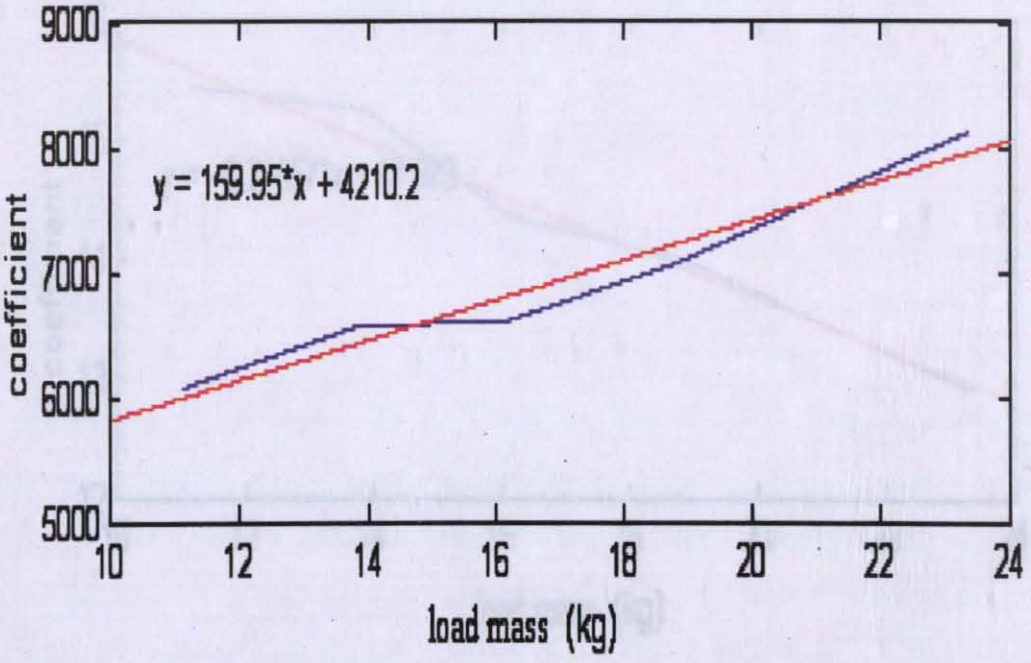

Figure 4.44 Coefficient b_1 (kgf/m^2) for relaxation related to mass (kg). Blue: experimental data, red: model's values.

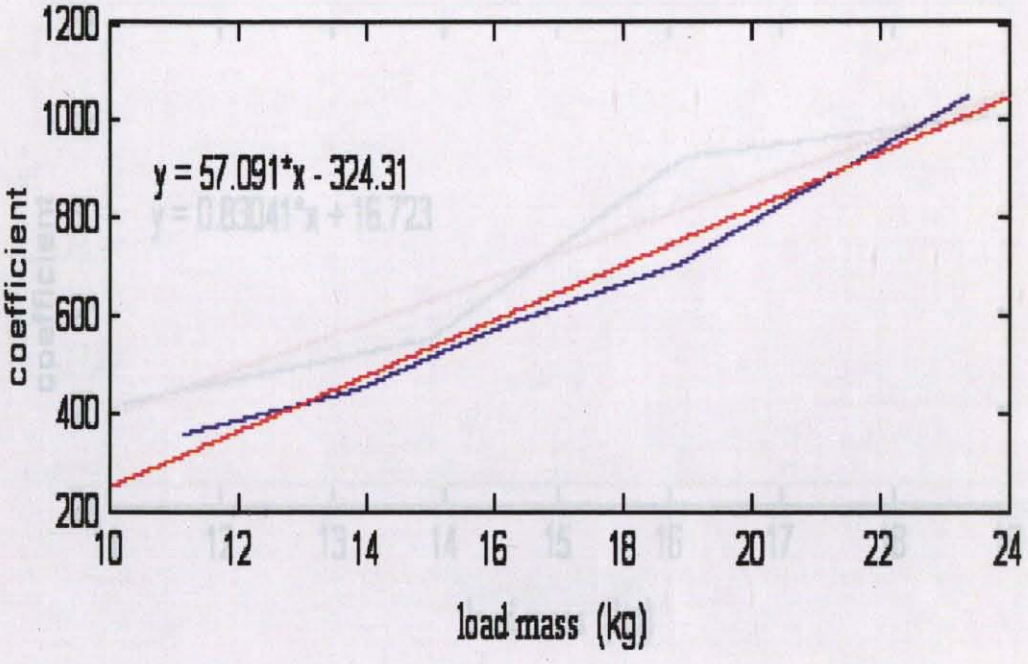

Figure 4.45 Coefficient b_2 (kgf/m^2) for relaxation related to mass (kg). Blue: experimental data, red: model's values.

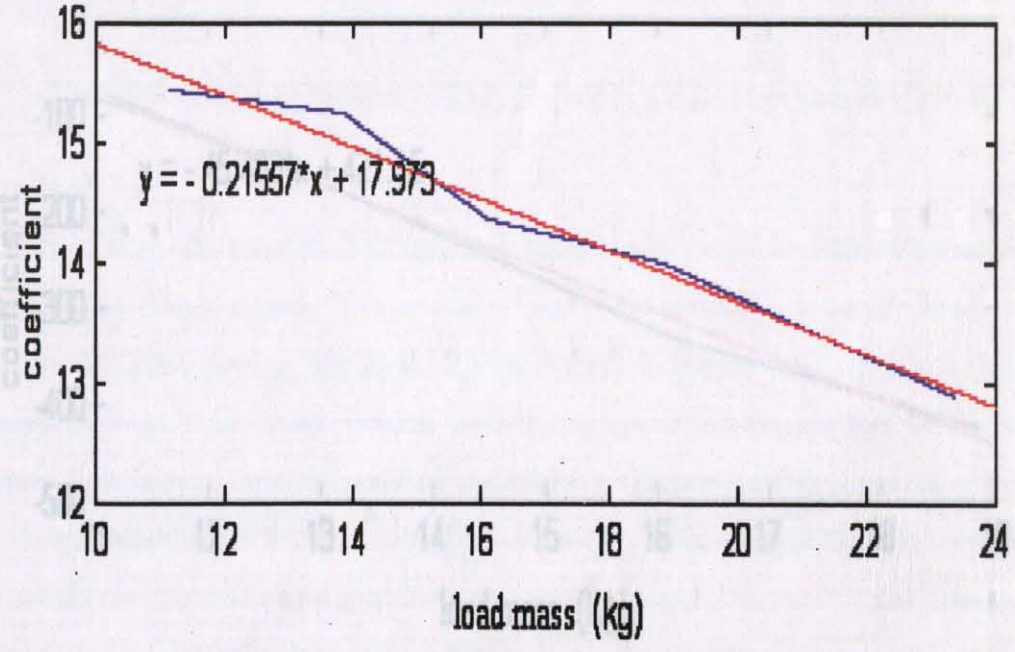

Figure 4.46 Coefficient b_3 (kgf/m^2) for relaxation related to mass (kg). Blue: experimental data, red: model's values.

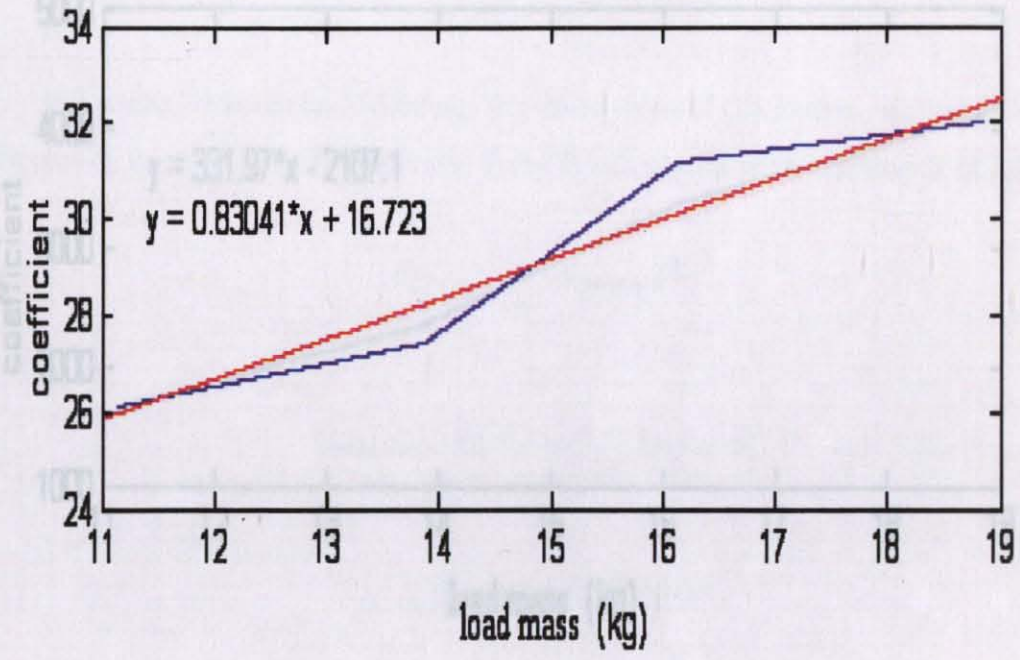

Figure 4.47 Coefficient b_4^0 (kgf/m^2 $(sec/mA)^2$) for relaxation related to mass (kg). Blue: experimental data, red: model's values.

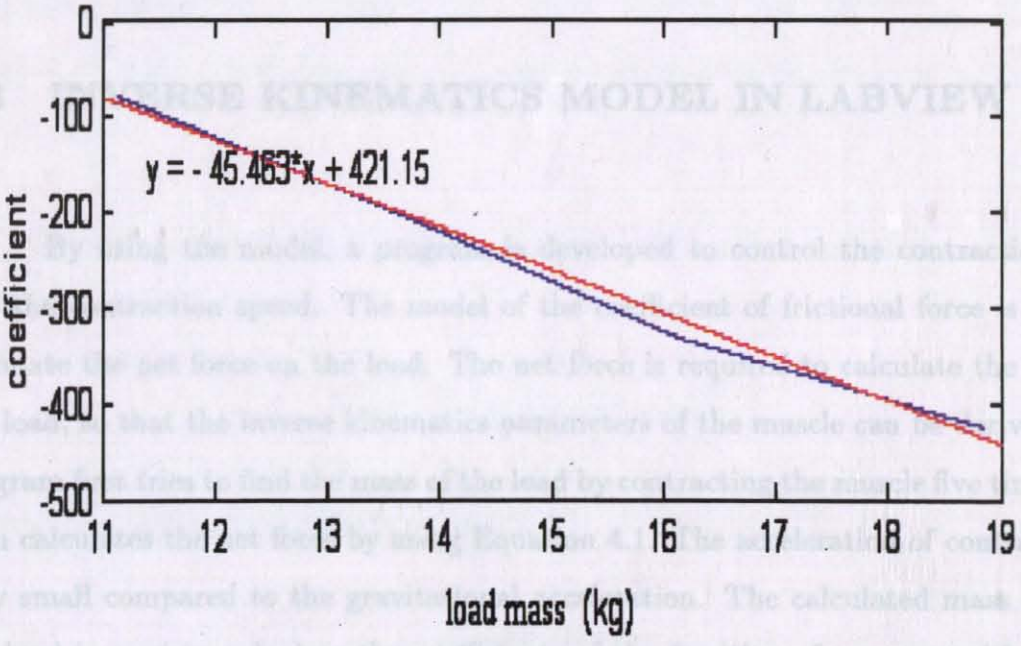

Figure 4.48 Coefficient b_4^1 (kgf/m^2 sec/mA) for relaxation related to mass (kg). Blue: experimental data, red: model's values.

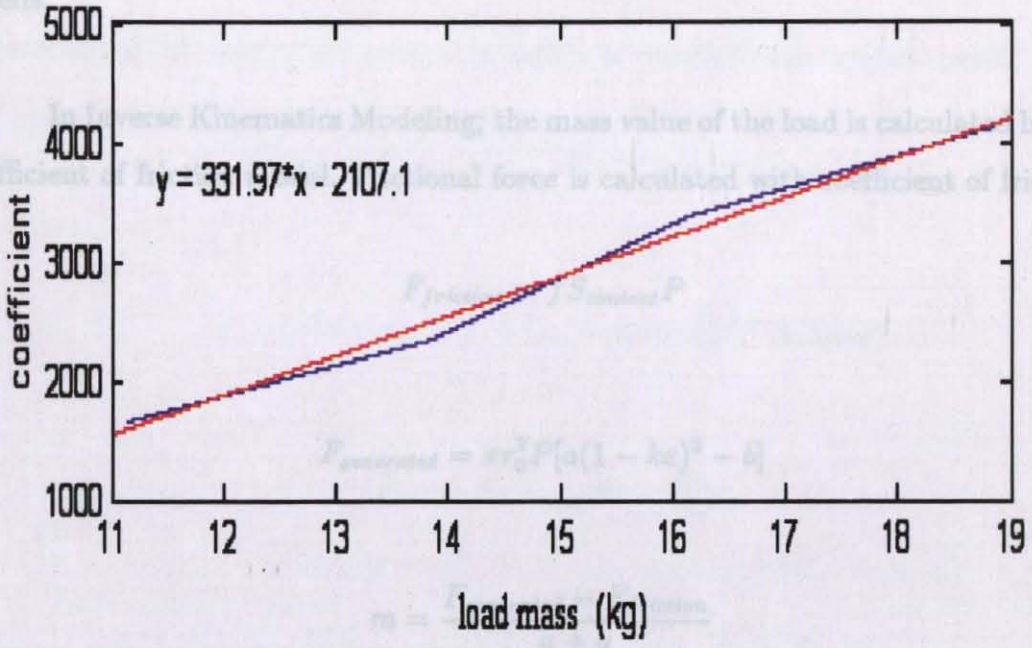

Figure 4.49 Coefficient b_4^2 (kgf/m^2) for relaxation related to mass (kg). Blue: experimental data, red: model's values.

4.3 INVERSE KINEMATICS MODEL IN LABVIEW

By using the model, a program is developed to control the contraction ratio and the contraction speed. The model of the coefficient of frictional force is used to calculate the net force on the load. The net force is required to calculate the mass of the load, so that the inverse kinematics parameters of the muscle can be derived. The program first tries to find the mass of the load by contracting the muscle five times, and then calculates the net force by using Equation 4.1. The acceleration of contraction is very small compared to the gravitational acceleration. The calculated mass value of the load is used to calculate the coefficients of the function of pressure with respect to the contraction ratio. For the target contraction ratio and the target contraction speed; the pressure and the current speed are calculated by the program. Finally, the

program finds the error for 30 different contraction ratios and 5 different contraction speeds.

In Inverse Kinematics Modeling; the mass value of the load is calculated by using coefficient of friction model. Frictional force is calculated with coefficient of friction.

$$F_{friction} = f S_{contact} P \tag{4.29}$$

$$F_{generated} = \pi r_0^2 P[a(1 - k\varepsilon)^2 - b] \tag{4.30}$$

$$m = \frac{F_{generated} - F_{friction}}{a + g} \tag{4.31}$$

where; f is the coefficient of friction, a is the acceleration, and m is the mass.

The mass value, target contraction ratio, and contraction speed are used to calculate the needed pressure and electrical current speed values. The triangle waveform of electrical current has constant current speed, and the pressure is proportional to electrical current. Thus, the rate of change of pressure is proportional to electrical current speed.

The extraction of the inverse kinematics modeling formulas for contraction of rubbertuator is as follows:

$$P = a_0 + a_1\varepsilon + a_2 e^{a_3\varepsilon} + a_4 ln\varepsilon \tag{4.32}$$

where; a_0, a_3, and a_4 depend only on mass.

$$a_1 = a_1^0 \nu + a_1^1 \tag{4.33}$$

$$a_2 = a_2^0 \nu + a_2^1 \tag{4.34}$$

where; a_1^0, a_1^1, a_2^0, and a_2^1 are constants, and ν is the electrical current speed.

$$P = a_0 + a_1^0 \nu\varepsilon + a_1^1 \varepsilon + a_2^0 \nu e^{a_3\varepsilon} + a_2^1 e^{a_3\varepsilon} + a_4 ln\varepsilon \tag{4.35}$$

$$P = (a_1^0 \varepsilon + a_2^0 e^{a_3\varepsilon})\nu + (a_0 + a_1^1 \varepsilon + a_2^1 e^{a_3\varepsilon} + a_4 ln\varepsilon) \tag{4.36}$$

$$\dot{P} = (a_1 + a_2 a_3 e^{a_3\varepsilon} + \frac{a_4}{\varepsilon})\dot{\varepsilon} \tag{4.37}$$

$$\dot{P} = (a_1^0 \nu + a_1^1 + a_2^0 a_3 \nu e^{a_3\varepsilon} + a_2^1 a_3 e^{a_3\varepsilon} + \frac{a_4}{\varepsilon})\dot{\varepsilon} \tag{4.38}$$

Pressure is directly proportional to electrical current as in Figure 3.5. Hence, pressure speed ($\dot{P}$) is proportional to electrical current speed (ν). For the target trajectory and known mass, the constants in the Equation 4.38 are found, and the current speed for the target trajectory is extracted. After finding the current speed, the pressure that is needed for target trajectory is calculated with the Equation 4.36.

The extraction of the inverse kinematics modeling formulas for relaxation of rubbertuator is as follows:

$$P = b_0 + b_1 \varepsilon + b_2 e^{b_3\varepsilon} + b_4 ln\varepsilon \tag{4.39}$$

where; b_1, b_2, and b_3 depend only on mass.

$$b_0 = b_0^0 \nu + b_0^1 \tag{4.40}$$

$$b_4 = b_4^0 \nu^2 + b_4^1 \nu + b_4^2 \tag{4.41}$$

where; b_0^0, b_0^1, b_4^0, b_4^1 and b_4^2 are constants, and ν is the electrical current speed.

$$P = b_0^0\nu + b_0^1 + b_1\varepsilon + b_2e^{b_3\varepsilon} + b_4^0\nu^2 ln\varepsilon + b_4^1\nu ln\varepsilon + b_4^2 ln\varepsilon \tag{4.42}$$

$$P = b_4^0 ln\varepsilon\nu^2 + (b_0^0 + b_4^1 ln\varepsilon)\nu + (b_0^1 + b_1\varepsilon + b_2e^{b_3\varepsilon} + b_4^2 ln\varepsilon) \tag{4.43}$$

$$\dot{P} = (b_1 + b_2b_3e^{b_3\varepsilon} + \frac{b_4}{\varepsilon})\dot{\varepsilon} \tag{4.44}$$

$$\dot{P} = (b_1 + b_2b_3e^{b_3\varepsilon} + \frac{b_4^0}{\varepsilon}\nu^2 + \frac{b_4^1}{\varepsilon}\nu + \frac{b_4^2}{\varepsilon})\dot{\varepsilon} \tag{4.45}$$

Pressure is directly proportional to electrical current as in Figure 3.5. Hence, pressure speed ($\dot{P}$) is proportional to electrical current speed (ν). For the target trajectory and known mass, the constants in the Equation 4.45 are found, and electrical current speed for the target trajectory is extracted. After finding the electrical current speed, the pressure that is needed for target trajectory is calculated with the Equation 4.43.

The inverse kinematics model is used to control the muscle's contraction ratio and the contraction speed. The mass of the load for the experiments is 8.87 kg. However, the program measured the mass, 9.45 kg, thus the percentage error is 6.5. The errors in contraction ratio and contraction speed are mapped for different contraction ratio and contraction speeds in Figures 4.50 and 4.51:

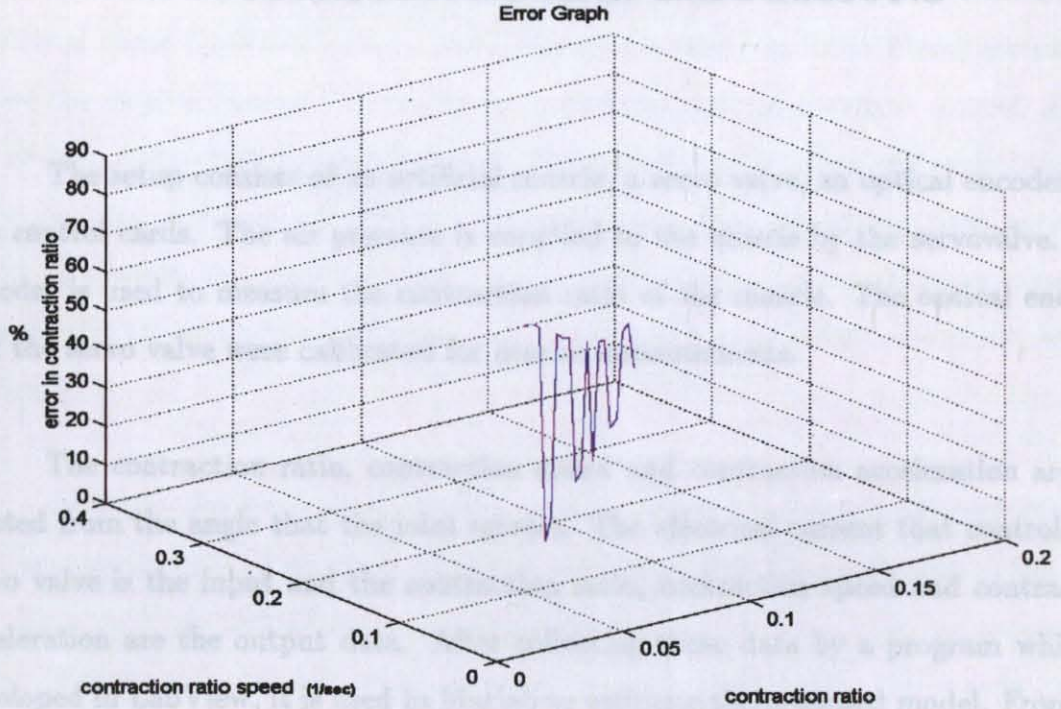

Figure 4.50 Error map of the target contraction ratio for the target 0 contraction speed (meter per second).

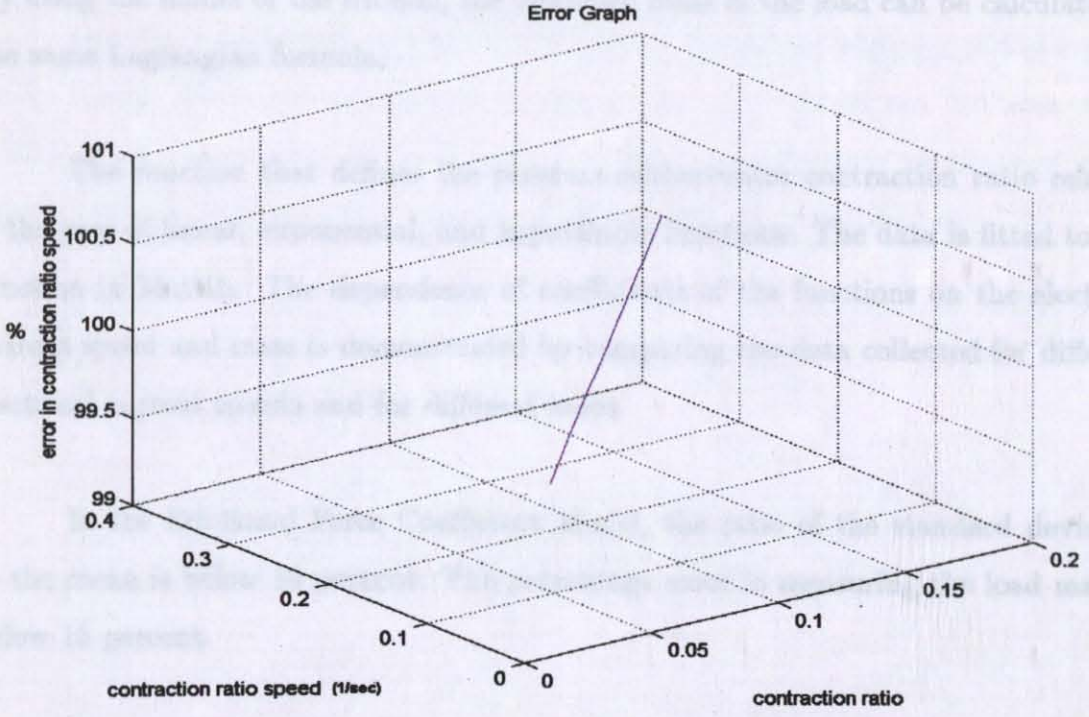

Figure 4.51 Error map of the target contraction ratio speed for the target 0 contraction speed (meter per second).

5. CONCLUSIONS AND DISCUSSIONS

The setup consists of an artificial muscle, a servo valve, an optical encoder and two control cards. The air pressure is supplied to the muscle by the servovalve. The encoder is used to measure the contraction ratio of the muscle. The optical encoder and the servo valve were calibrated for precise measurements.

The contraction ratio, contraction speed and contraction acceleration are extracted from the angle that the joint rotates. The electrical current that controls the servo valve is the input and the contraction ratio, contraction speed and contraction acceleration are the output data. After collecting those data by a program which is developed in LabView, it is used in Matlab to estimate the proposed model. From the Lagrangian equation of the system, it is seen that the coefficient of friction between the threads depends on the contraction ratio and the electrical current speed. The function that defines this relation is a superposition of linear and logarithmic functions. By using the model of the friction, the unknown mass of the load can be calculated in the same Lagrangian formula.

The function that defines the pressure-rubbertuator contraction ratio relation is the sum of linear, exponential, and logarithmic functions. The data is fitted to this function in Matlab. The dependence of coefficients of the functions on the electrical current speed and mass is demonstrated by comparing the data collected for different electrical current speeds and for different loads.

In the Frictional Force Coefficient Model, the ratio of the standard deviation to the mean is below 10 percent. The percentage error in measuring the load mass is below 15 percent.

In the Pressure-Contraction Ratio Model, the ratio of the standard deviation to the mean is below 15 percent.

Finally, by using both models, a control system is designed. The functions of the Frictional Force Coefficient Model and Pressure-Contraction Ratio Model are used to derive the Inverse Kinematics Functions to perform load independent control. Before the system is activated, the user enters parameters of the target trajectory; contraction ratio and contraction speed. To yield the target trajectory, the system finds necessary electrical current and current speed. As the system is run for an unknown mass, the system first calculates the load mass and then finds the coefficients which depend on the mass.

However, the system calculates necessary electrical current and current speed with an unacceptable large error. The error may arise from the constraints of the muscle. For a targeted contraction ratio of the muscle, there is a limit for the contraction speed. For example, around zero or maximum contraction ratio, the muscle cannot react fast. If the target trajectory is not between these limits, it is unavoidable to run the system with a large error. The modification of derivation of the Inverse Kinematics functions regarding the physical limits may lead to more accurate results.

Despite these errors, the model explains the non-linear behavior of the muscle. Its hysteresis depends on a number of parameters. The model can be achieved by taking those parameters into consideration. The thermodynamic parameters of the muscle may be helpful because the muscle is actuated by pressurized air.

REFERENCES

1. Medrano-Cerda G. A., C. J. Bowler, D. G. Caldwell: "Adaptive Position Control of Antagonistic Pneumatic Muscle Actuators," *IEEE International Conference on Intelligent Robots and Systems*, Vol. 1, pp. 378-383, 1995.

2. Morton W. E. and J. Hearle, *Physical Properties of Textile Fibres*, The Textile Institute, Manchester, 1962.

3. Tondu B., and P. Lopez, "Modeling and Control of McKibben Artificial Muscle Robot Actuators," *IEEE Control System Magazine*, Vol. 20, pp. 15-38, April 2000.

4. Chou C. P., B. Hannaford, "Static and Dynamic Characteristics of McKibben Pneumatic Artificial Muscles," *Proceedings of IEEE International Conference on Robotics and Automation*, San Diego, CA, May 1994.

5. ACFAS Dept, *Servo Rubbertuator Kit Operational Manual*, Bridgestone Corporation, Japan.

6. Tondu P., and P. Lopez, "The McKibben Muscle and its Use in Actuating Robot Arms Showing Similarities with Human Arm Behavior," *Industrial Robot*, Vol. 24, no. 6, pp. 432-439, 1997.

7. Thongchai S., M. Goldfarb, N. Sarkar, and K. Kawamura, "A Frequency Modeling Method of Rubbertuators for Control Application in an IMA Framework," *Proceedings of American Control Conference*, Arlington, 25-27 June 2001, pp. 1710-1714, Virginia, June 2001.

8. Klute G. K., and B. Hannaford, "Fatique Characteristics of McKibben Artificial Muscle Actuators," *Proceedings of IEEE/RSJ 1998 International Conference on Intelligent Robotic Systems (IROS '98)*, Victoria BC, Canada, Nov. 1998.

9. Klute G. K., and B. Hannaford, "Accounting for Elastic Energy Storage in McKibben Artificial Muscle Actuators," *ASME Journal of Dynamic Systems, Measurement, and Control*, Vol. 122, pp. 386-388, June 2000.

10. Klute, G. K., J. Czerniecki, and B. Hannaford, "McKibben Artificial Muscles: Actuators with Biomechanical Intelligence," *Proceedings of the IEEE/ASME 1999 International Conference on Advanced Intelligent Mechatronics (AIM '99)*, Atlanta, GA, Sept. 19-23, 1999, pp. 221-226.

11. Ozkan M., K. Inoue, K. Negishi, T. Yamanaka, "Defining a Neural Network Controller Structure for a Rubbertuator Robot," *Neural Networks*, Vol. 13, pp. 533-544, 2000.

12. Eskiizmirliler S., N. Forestier, B. Tondu, C. Darlot, "A Model of the Cerebellar Pathways Applied to the Control of a Mobile Mechanical Segment," *Biological Cybernetics*, Vol. 86, no. 5, pp. 379-394, 2002.